

Self-trapped states in BaBiO_3

A Thesis Presented

by

Ilka Bettina Bischofs

to

The Graduate School

in Partial Fulfillment of the Requirements

for the Degree of

Master of Arts

in

Physics

State University of New York

at

Stony Brook

December 2000

Copyright © by
Ilka Bettina Bischofs
2000

State University of New York
at Stony Brook

The Graduate School

Ilka Bettina Bischofs

We, the thesis committee for the above candidate for the
Master of Arts degree,
hereby recommend acceptance of the thesis.

Dr. Philip B. Allen

Advisor

Professor of Physics, Department of Physics and Astronomy

Dr. Peter W. Stephens

Professor of Physics, Department of Physics and Astronomy

Dr. Peter van Nieuwenhuizen

Professor of Physics, Department of Physics and Astronomy

Dr. Christie S. Nelson

Department of Physics,

Brookhaven National Laboratory

This thesis is accepted by the Graduate School.

Dean of the Graduate School

Contents

List of Figures	vii
Chapter 1 Introduction	1
1.1 Material properties of the BaBiO ₃ family	1
1.2 Mechanism for HTSC and MI-transition	3
1.3 Thesis goals	4
Chapter 2 The Rice-Sneddon model	6
2.1 The model Hamiltonian	6
2.1.1 The generic Hamiltonian	6
2.1.2 Simplifications	8
2.2 Algorithm for the numerical studies	10
2.2.1 Derivation of the force \vec{F} -expression	11
2.2.2 The variable metric method	11
2.2.3 Matrix diagonalization	13
2.2.4 Summary and further details	15
Chapter 3 The Peierls insulator BaBiO₃	17

3.1	Introduction: 1D-metal-insulator transitions	17
3.2	The extremes: $g \rightarrow 0$ and $t \rightarrow 0$	20
3.2.1	Delocalized electron states: $g = 0$	20
3.2.2	Localized electron states: $t = 0$	20
3.3	Analytical studies of the CDW instability for a half-filled band	21
3.3.1	Opening of the Peierls gap	22
3.3.2	Self-consistent determination of the ODW- and CDW-amplitudes	25
3.3.3	Artifacts of the model	27
3.4	Numerical results	28
3.4.1	Notes on the numerical calculations	28
3.4.2	Hopping versus electron-phonon-term: competition and compromise in the half-filled case	28
3.5	Experiment and theory	33
3.5.1	Experimental results	33
3.5.2	Determination of Γ and comparison between theory and experiment	34

Chapter 4 Light doping of the charge-ordered state: polaron and bipolaron formation 36

4.1	Introduction	36
4.1.1	Theories for the MI-transition under doping	36
4.1.2	General introduction to polaron theory	38
4.1.3	The RS-model: self-trapping in the empty band case	40

4.2	The idea of self-trapping on the background of the charge-ordered state	42
4.2.1	Polaron formation in the $t = 0$ case	42
4.2.2	Bipolaron formation in the $t = 0$ case	43
4.2.3	The effect of hopping $t \neq 0$	44
4.3	Numerical results	45
4.3.1	Notes on the numerical calculations	45
4.3.2	Stability of self-trapped states	46
4.3.3	Analysis: continuous transition from a small to large polaron	52
4.4	Summary and conclusions	64
4.4.1	Toyozawa criterion for self-trapping in the half-filled band	64
4.4.2	Bipolarons in the BBO-system	66
Chapter 5 Excitations across the Peierls gap		68
5.1	Introduction	68
5.2	Low lying excitations in the charge-ordered system	71
5.2.1	Weak electron-phonon coupling: CDW-picture	71
5.2.2	Strong electron-phonon coupling: bipolaronic crystal picture	71
5.3	Numerical results	75
5.3.1	Notes on the numerical calculations	75
5.3.2	Existence of relaxed excited states	76
5.3.3	Nature of the relaxed excited states	78
5.4	Conclusions	79

Chapter 6	Manifestation of self-trapped states in experiment	82
6.1	Introduction	82
6.2	The half-filled band	83
6.2.1	DOS-effect	83
6.2.2	Franck-Condon effect: signature of the ST-exciton . . .	86
6.2.3	Experimental impact and comparison to experiment . .	91
	Bibliography	94

List of Figures

1.1	Cubic perovskite structure ABX_3 : crystal structure of superconducting BKBO and BPbBO	2
2.1	The RS-Model	8
3.1	Density of states for $\Gamma = 0.3$, evaluated with a tetrahedron code [30][31] (line) together with a histogram obtained by diagonalizing H for a super-cell with 1020 Bi atoms	25
3.2	Γ -dependence of the system energy per atom E_{tot} , E_L and E_e , arrows indicate Γ_{c1} and Γ_{c2}	31
3.3	Γ -dependence of Δ and the CDW-amplitude ρ_0	32
4.1	Polaron lattice relaxation energy ϵ_p	49
4.2	Bipolaron lattice relaxation energy ϵ_b	51
4.3	Polaron and bipolaron binding energies normalized to the gap Δ	53
4.4	Charge localized on the center of the (bi)polaron	55
4.5	Total induced excess charge	57
4.6	Exponential decay and CDW-character of the polarons	58
4.7	Gap state energy dependence on Γ	61
4.8	Localization of gap states: IPR computed for the polaron	64

4.9	Thermally assisted hopping motion of a small bipolaron, black: Bi ⁺⁵ , white: Bi ⁺³ , grey: Bi ⁺⁴	67
5.1	The self-trapped exciton, black: Bi ⁵⁺ , grey: Bi ⁴⁺ , white: Bi ³⁺	73
5.2	Potential energy of ground state and excited state at $t = 0$. .	75
5.3	Exciton lattice relaxation energy	77
5.4	Exciton gap states	79
5.5	Radius of exciton-hole and exciton-electron wave function and IPR's of the gap states	80
6.1	ϵ_2 in the RS-model without taking lattice polarization effects into account	85
6.2	Franck-Condon type spectra for the self-trapped exciton . . .	90
6.3	First temperature correction to ϵ_2	91

Chapter 1

Introduction

1.1 Material properties of the BaBiO_3 family

The discovery of high- T_c superconductivity in copper oxides renewed the interest in superconducting oxides up to the present day. Among these materials BaBiO_3 (BBO) and its related hole doped compounds – potassium (K) inserted in barium (Ba) sites $\text{Ba}_{1-x}\text{K}_x\text{BiO}_3$ and lead (Pb) in bismuth (Bi) sites $\text{BaPb}_x\text{Bi}_{1-x}\text{O}_3$ – is the object of a long-standing controversy. One of the most attractive feature of the BBO family is the existence of the highest T_c 's for non-copper based superconductors, except for alkali-metal doped C_{60} . For optimal doping with Pb the transition temperature is 13K, when doped with potassium the highest T_c is around 30K [1], [2]. These T_c values are exceptionally high in relation to the low density of electronic states at the Fermi level obtained from tunneling measurements [3]-[5]. Like the cuprates, the bismuthates exhibit a metal-to-insulator phase transition. The parent compound BaBiO_3 is an insulator and remains insulating up to a critical hole

concentration $x = 0.35$ for K-doping and $x = 0.65$ for Pb-doping, where the material becomes metallic/superconducting. The maximum transition temperature of T_c is reached at the MI-phase-boundary followed by decrease in T_c with over-doping [1]. Besides some other similarities, there are important differences between the BBO-materials the high- T_c copper-oxides as well. Although both materials are based on a perovskite type structure, the crystal structure of superconducting phase in the BBO is a cubic perovskite [6] accounting for isotropic superconductivity. This clearly differs from the layered two-dimensional CuO_2 structure typical for the cuprate. The charge carriers in the metallic compounds in BBO are electrons [7], [8] while in copper oxide they are holes. Moreover, the undoped BBO (as well as BKBO) is diamagnetic [9] [10] contrary to the anti-ferromagnetic ordering of CuO-compounds. Finally, a strong oxygen-isotope shift is observed for the superconductivity in BBO compared to much smaller values in copper oxides [11], [12].

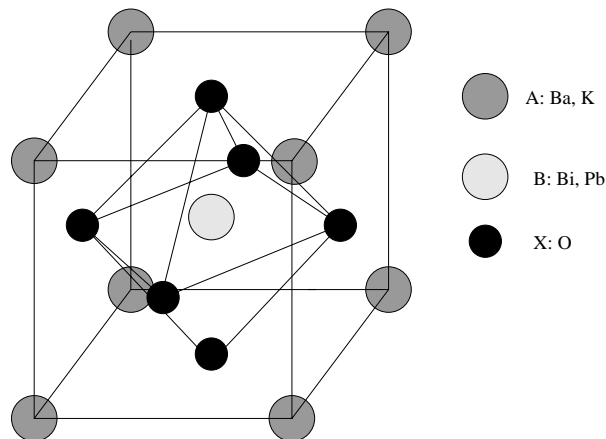


Figure 1.1: Cubic perovskite structure ABX_3 : crystal structure of superconducting BKBO and BPbBO

1.2 Mechanism for HTSC and MI-transition

The question whether a global mechanism for high- T_c superconductivity both for cuprate and BBO exists has still not been answered satisfactorily. HTSC in the copper-oxides is believed to be crucially related to strong electron-correlations of the Cu d electrons in the Cu-O band, crossing the Fermi energy. From band-structure calculations the valence band in the Bi-oxides is a dispersive Bi-O band made of Bi $6s$ and anti-bonded with O $2p$ states [13],[14]. Therefore, the Bi-atoms are regarded to play the role of the Cu-atoms. The larger size of the Bi $6s$ orbital leads to a smaller on-site Coulomb repulsion and a larger band-width. Thus, the material does not exhibit a Hubbard instability and it seems unlikely that strong electron-electron interaction plays a major role in the BBO-family. This would also imply that the origin of superconductivity is different in both materials. Supported by the strong isotope effect, a conventional phonon based pairing mechanism seems more likely in the BBO family, although the low density of states at the Fermi energy is unfavorable for BCS-type superconductivity.

Further evidence for the importance of electron-phonon coupling in the bismuthate comes from the MI-transition. The transition coincides with a structural change of the perfect cubic perovskite ($Pm\bar{3}m$) of the superconducting phase to an orthorhombic lattice ($Ibmm$) for $0.12 < x < 0.35$ (K-doping). Below $x = 0.12$ the lattice is monoclinic ($I2/m$). The later structures can be obtained from the cubic phase by successively introducing tilting of the oxygen-octrahedra (orthorhombic) plus alternating symmetric breathing-in and breathing-out distortions of the oxygens [6]. These structural distortions seem to be responsible for the insulating behavior of the parent com-

pound BaBiO_3 , which would be expected to be metallic in a perfect cubic environment.

It is reasonable to suppose that the electron-phonon interaction is responsible both for superconductivity and for keeping carriers trapped in the doped insulating phases. Since the MI-transition is coupled to the highest T_c values, insight in one mechanism will help to understand the other phenomenon as well. Both states – normal and superconducting– are still under active experimental and theoretical investigation.

1.3 Thesis goals

The present work concentrates on the insulating state properties of the bismuthate. The goal is to provide some contribution to understand the MI-transition in the BBO-family which is believed to be based primarily on electron-phonon interaction. For this purpose a simple model is studied numerically. The model is a simplified version of the Rice-Sneddon model and includes the band-motion of the Bi 6s-electrons and the electron-phonon term. It was introduced by Rice and Sneddon [16],[17] and will be presented together with the algorithm for the numerical calculations in the next chapter. The insulating behavior of BaBiO_3 is the topic of the third chapter. It can be interpreted in terms of a charge-ordered Peierls insulator. The analytical solution for the ground state is reviewed and the corresponding numerical results are shown.

Chapter four studies the insertion of holes as a model for the lightly doped material. Trapping of charge carriers in small polaron or bipolaron states will be the important concept. In chapter five the low-lying excitations

of the undoped material, i.e. the formation of self-trapped excitons, is investigated numerically. Finally in chapter six, the impact of the electron-phonon interaction on the optical properties is discussed. In each chapter comparisons of the model predictions with experiments will be made. However, due to the simplicity of the model only qualitative agreement is expected. The question is whether this simple model describes the relevant physics of the material correctly.

Chapter 2

The Rice-Sneddon model

2.1 The model Hamiltonian

2.1.1 The generic Hamiltonian

In the ideal cubic perovskite structure (Fig.1.1) the cation in the center B is surrounded by six oxygen anions X . Charges localized on the B cation interact via Coulomb forces with the oxygens anions and thus can cause them to move lowering the total energy of the system. The energy to displace an oxygen is determined by the charge difference $n_l - n_{l+1}$ between adjacent B sites and strain energy:

$$E_{l,l+1} = \frac{1}{2}Ku^2 - gu(n_l - n_{l+1}), \quad (2.1)$$

where K is the elastic constant, u the displacement and g a coupling constant. A quantum mechanical model describing this effect must take into account which B -atom orbitals are occupied, the electron-lattice coupling and the electron-electron correlations. Thus, the generic Hamiltonian, first intro-

duced by Rice and Sneddon [16], reads:

$$H = H_t + H_{e-ph} + H_{ph} + H_C, \quad (2.2)$$

where H_t , H_{e-ph} , H_{ph} and H_C are, correspondingly, the hopping, electron-phonon, phonon and Coulomb terms.

The BBO-family has a fairly simple set of valence electron states. The conduction band consists of Bi 6s antibonded with O 2p-states. It is minimally affected by substituting K in Ba sites [14],[18], which justifies the use of the same band-structure model for the undoped and doped material. The model keeps only one electronic degree of freedom, the Bi 6s amplitude with effective hopping only to next neighbor bismuth neighbors:

$$H_t = -t \sum_{\langle l,l' \rangle, \sigma} c_{l,\sigma}^\dagger c_{l',\sigma}. \quad (2.3)$$

Displacements of the oxygens along the direction of the Bi-O bonds couple strongly to the Bi 6s electron states. The important lattice degree of freedom is therefore believed to be the breathing mode distortion of the oxygens. The oxygens are treated as Einstein oscillators with frequency ω_0 :

$$H_{ph} = \sum_{l,\alpha} \left(\frac{1}{2} M \omega_0^2 u^2(l, \alpha) + \frac{P_{l,\alpha}^2}{2M} \right). \quad (2.4)$$

Coupling between electrons and phonons is incorporated through the term:

$$H_{e-ph} = \frac{g}{\alpha} \sum_{l,\sigma} e(l) c_{l,\sigma}^\dagger c_{l,\sigma}. \quad (2.5)$$

$e(l)$ is the local breathing amplitude on the l -th Bi atom, defined as:

$$e(l) = \sum_{\alpha=x,y,z} u(l, +, \alpha) - u(l, -, \alpha) \quad (2.6)$$

The notation $u(l, \pm, \alpha)$ refers to the displacement of the oxygen atom located $\vec{R}_l \pm (\frac{a}{2})\hat{\alpha}$ with $\hat{\alpha} = x, y, z$ the Cartesian directions, a the pseudo-cubic lattice constant and \vec{R}_l the position of the l 's Bi atom. Finally, the electron-electron correlations interact via intra- and inter-site Coulomb interaction:

$$H_C = U \sum_l n_{l,\uparrow} n_{l,\downarrow} + \sum_{l \neq l', \sigma, \sigma'} \frac{e^2}{\epsilon |\vec{R}_l - \vec{R}_{l'}|} n_{l\sigma} n_{l'\sigma'} \quad (2.7)$$

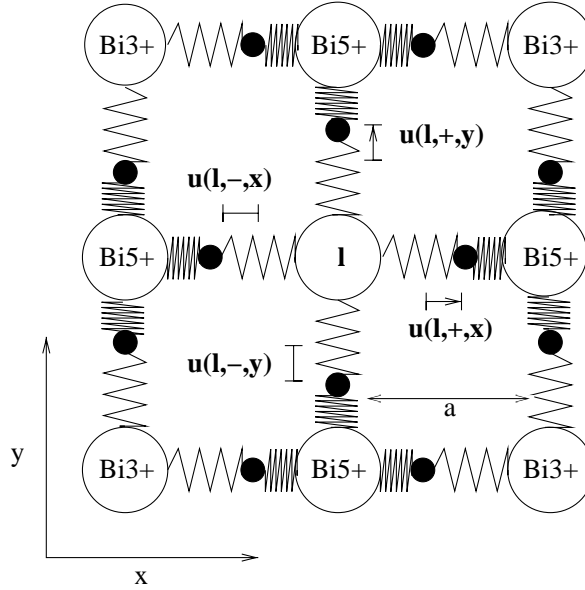


Figure 2.1: The RS-Model

2.1.2 Simplifications

The RS-Hamiltonian has been studied under various aspects, in several limits and with different simplifications [19]-[21]. The original paper by Rice and

Sneddon [16] treated the problem in the $t \rightarrow 0$ limit and concluded that electrons in BaBiO₃ could pair in real space (negative effective U). Each Bi-atom contributes one electron to the system and the nominal valence of Bi is 4+. Due to the interaction with the lattice, the lattice interaction can overcome the Hubbard U repulsion leading to an effective negative U , which causes the charges to disproportionate:



Electron correlations become important in narrow bands, as the time τ an electron spends on a site is related to the band-width W by $\tau = \frac{\hbar}{W}$. The valence band is quite broad, so that in our implementation we treat the opposite case. The electron-electron interactions are neglected and the hopping term is taken into account.

Furthermore, since the electron motion is much faster than the motion of the oxygen atoms, the oxygens are treated adiabatically. The kinetic energy in H_{ph} is ignored, and the displacements are approximated as classical stationary parameters. The size of non-adiabatic effects is governed by $\hbar\omega_0/t$. Mass M and frequency ω_0 of the Einstein oscillators determine the spring constant $K = M\omega_0^2$.

In conclusion, our Hamiltonian reads:

$$H = -t \sum_{\langle l,l'\rangle,\sigma} c_{l,\sigma}^\dagger c_{l',\sigma} - g \sum_{l,\sigma} e(l) c_{l,\sigma}^\dagger c_{l,\sigma} + \sum_{l,\alpha} \frac{1}{2} K u^2(l, \alpha). \quad (2.9)$$

The physics of this Hamiltonian is controlled by one dimensionless parameter Γ :

$$\Gamma = \frac{g^2}{Kt}, \quad (2.10)$$

that governs the electron-phonon effects. The energy is conveniently measured in units of t and oxygen-displacements in units of $u_0 = \sqrt{(t/K)}$. Using the scaled Hamiltonian $\tilde{H} = H/t$ and the scaled displacements \tilde{e} the Hamiltonian rewrites:

$$\tilde{H} = - \sum_{\langle l,l' \rangle, \sigma} c_{l,\sigma}^\dagger c_{l',\sigma} - \sqrt{\Gamma} \sum_{l,\sigma} \tilde{e}(l) c_{l,\sigma}^\dagger c_{l,\sigma} + \sum_{l,\alpha} \frac{1}{2} \tilde{u}^2(l, \alpha) \quad (2.11)$$

2.2 Algorithm for the numerical studies

The Hamiltonian (2.11) can be studied analytically only in very special cases, e.g. in the case of a half-filled Bi-band. For all other studies, e.g. doped ground-state solutions or calculations of excited states, numerical methods have to be applied. For the numerical studies in this work, a finite cluster containing N Bi atoms is chosen and the scaled Hamiltonian is diagonalized exactly using periodic boundary conditions. The positions u_l of the oxygens are treated as $3N$ independent parameters. Thus, the total energy is a function of \vec{u} , a $3N$ dimensional vector containing the scaled oxygen displacements $\vec{u} = (u_1, \dots, u_l, \dots, u_{3N})$:

$$E_{\text{tot}}(\vec{u}) = E_e(\vec{u}) + E_L(\vec{u}) = \sum_{\text{occ}} \epsilon_i(\vec{u}) + \frac{1}{2} \vec{u} * \vec{u}. \quad (2.12)$$

E_e is the electronic part of the total energy, obtained by occupying the relevant states i with energy ϵ_i , and E_L the elastic energy costs.

In order to find the ground state, the total energy has to be minimized with respect to the u_l . This is a multidimensional minimization problem which can be solved with several algorithms. Most of them require the knowledge of the function's gradient- in our case the force vector \vec{F} , containing the forces $F(l)$ acting on the l -th oxygen. The expression for \vec{F} can be easily derived.

2.2.1 Derivation of the force \vec{F} -expression

The force $F(l)$ acting on the l -th oxygen along the Bi-O bond is given by:

$$F(l) = -\frac{\partial E_{\text{tot}}}{\partial u_l} = F_L(l) + F_e(l) = -u_l - \frac{\partial}{\partial u_l} \left(\sum_{\text{occ}} \epsilon_i \{u\} \right) \quad (2.13)$$

F_e can be evaluated using the eigenvectors Ψ_i projected on position eigenstates $|k\rangle$:

$$F_e(l) = \frac{\partial}{\partial u_l} \sum_{i,\text{occ}} \epsilon_i \{u\} = \frac{\partial}{\partial u_l} \sum_{i,\text{occ}} \sum_{k,k'} \langle \Psi_i | k \rangle \langle k | H | k' \rangle \langle k' | \Psi_i \rangle. \quad (2.14)$$

The derivative has to be evaluated with the product rule. Only the sum where the derivative acts on the matrix elements will contribute, since the other two sums add up to zero using $H|\Psi_i\rangle = \epsilon_i|\Psi_i\rangle$ and $\langle \Psi_i | \Psi_i \rangle = 1$.

Thus:

$$F_e(l) = - \sum_{i,\text{occ}} \sum_{k,k'} \langle \Psi_i | k \rangle \left(\frac{\partial}{\partial u_l} \langle k | H | k' \rangle \right) \langle k' | \Psi_i \rangle. \quad (2.15)$$

There are only two diagonal matrix elements that dependent on u_l . They correspond to the the Bi positions l and l' which are next to the l -th oxygen and read $\langle l | H | l \rangle = \sqrt{\Gamma} u_l$ and $\langle l' | H | l' \rangle = -\sqrt{\Gamma} u_l$, respectively. Therefore, the force can be finally written as:

$$F_{el}(l) = -\sqrt{\Gamma} \sum_{i,\text{occ}} (|\langle \Psi_i | l \rangle|^2 - |\langle \Psi_i | l' \rangle|^2). \quad (2.16)$$

This means that the force on an oxygen atom along a Bi-Bi bond is proportional to the charge difference between neighboring Bi atoms.

2.2.2 The variable metric method

Using the gradient information the variable metric method [22] was applied to find the optimal distortion vector \vec{u} .

This algorithm is sometimes called quasi-Newton method. It assumes that $E_{\text{tot}}(\vec{u})$ can be locally approximated by a 2nd order Taylor expansion:

$$E_{\text{tot}}(\vec{u}) = c - \vec{b} \cdot \vec{u} + \frac{1}{2!} \vec{u} \cdot \hat{A} \cdot \vec{u}, \quad (2.17)$$

where \hat{A} is the Hessian matrix or bare force matrix. The minimum point \vec{u}_m in Eq. (2.17) fulfills:

$$\hat{A} \cdot \vec{u}_m = \vec{b}. \quad (2.18)$$

On the other hand, at the current point \vec{u}_i we can write, using $F(\vec{u}_i) = -\nabla E_{\text{tot}}(\vec{u}_i) = \vec{b} - \hat{A} \cdot \vec{u}_i$:

$$\hat{A} \cdot \vec{u}_i = -\vec{F}(\vec{u}_i) + \vec{b}. \quad (2.19)$$

Subtracting (2.18) and (2.19) from each other and multiplying \hat{A}^{-1} from the right defines the finite step $\vec{u}_i - \vec{u}_m$ to get to the exact minimum:

$$\vec{u}_m - \vec{u}_i = \hat{A}^{-1} \cdot \vec{F}(\vec{u}_i) \quad (2.20)$$

Since \hat{A} is not known, the idea of the variable metric algorithm is to construct a recursive series \hat{H}_i converging against the inverse Hessian matrix \hat{A}^{-1} . The series \hat{H}_i is constructed according to the Davidon-Fletcher-Powell algorithm:

$$H_{i+1} = H_i + \frac{\Delta \vec{u}_i \otimes \Delta \vec{u}_i}{\Delta \vec{u}_i \cdot \Delta \vec{F}_i} - \frac{(\hat{H}_i \cdot \Delta \vec{u}_i) \otimes (\Delta \vec{F}_i \cdot \hat{H}_i)}{\Delta \vec{F}_i \cdot \hat{H}_i \cdot \Delta \vec{F}_i}. \quad (2.21)$$

\hat{H}_0 is initialized as a unit-matrix times the maximum force value of the starting point u_0 .

The optimal oxygen positions are then found iteratively:

$$\vec{u}_{i+1} = \vec{u}_i + \Delta \vec{u}_i \quad (2.22)$$

with

$$\Delta \vec{u}_i = \hat{H}_i \cdot \vec{u}_i. \quad (2.23)$$

This algorithm converges quadratically in the number of vector dimensions of \vec{u} for more general smooth functions.

2.2.3 Matrix diagonalization

For each iteration step i in the minimization algorithm, the new wave-functions have to be calculated to obtain the force \vec{F} . Thus in each step, the Hamiltonian has to be diagonalized with the corresponding oxygen-positions. For the diagonalization of the matrix, the TQLI-method (tridiagonal **QL**-algorithm with implicit shifts) was used and the code from the numerical recipes in C implemented [22].

The algorithm uses a set of similarity transformations S :

$$A' = SAS, \quad (2.24)$$

that leave the eigenvalues unchanged, to diagonalize the matrix.

In a first step the symmetric $n \times n$ matrix is reduced to a tridiagonal form T , by applying a series of $n-2$ orthogonal Householder transformations P_i . The tridiagonal matrix is then diagonalized iteratively using the QL-algorithm with implicit shifts. Finally the eigenvectors of the original matrix are obtained from the eigenvectors of T by applying the accumulated transformation:

$$P = P_1 P_2 P_3 \dots P_{n-2} \quad (2.25)$$

to those eigenvectors.

The idea behind the QL-algorithm is that any real matrix A can be decomposed in a form:

$$A = QL, \quad (2.26)$$

where Q is orthogonal and L is lower triangular.

The mathematical background of the algorithm is a theorem, which states, that in the sequence of orthogonal transformations:

$$A_s = Q_s L_s \quad (2.27)$$

$$A_{s+1} = L_s Q_s = Q_s^T A_s Q_s \quad (2.28)$$

A_s converges to lower triangular form and the eigenvalues λ_i of A appear on the diagonal in increasing order of absolute magnitude.

The convergence of the elements a_{ij}^s above the diagonal to zero is determined by :

$$a_{ij}^s \approx \left(\frac{\lambda_i}{\lambda_j}\right)^s \quad (2.29)$$

Therefore, the convergence can be slow if the eigenvalues lie close together. The convergence can be enhanced by the technique of shifting. Subtracting a matrix $k\hat{1}$ from A shifts the eigenvalues to $\lambda_i - k$ and thus the convergence is determined by the ratio:

$$\frac{\lambda_i - k}{\lambda_j - k}. \quad (2.30)$$

In order to maximize the convergence rate for each step s , k_s is computed by diagonalizing the leading 2x2 subdiagonal and k_s is chosen as the eigenvalue closer to a_{11} . The method of implicit shifts does not require k_s to be actually

subtracted from A , which is advantageous for the numerical accuracy. Instead the shifts enter implicitly, when constructing the orthogonal matrices Q_s .

Since $Q_s^T A_s = L_s$, Q_s consists of a product of $n - 1$ orthogonal matrices:

$$Q_s = P_1^s P_2^s \dots \tilde{P}_{n-1}^s, \quad (2.31)$$

designed to successively annihilate super-diagonal elements in A_s . In the case of implicit shifting, the P_i^s are Givens transformations and \tilde{P}_{n-1}^s is a plane rotation containing k_s as a parameter.

The workload of the TQLI- algorithm is about $30n^2$ for the diagonalization and a total operation count of $3n^3$ is needed, when both eigenvalues and eigenvectors are required. For our calculations the eigenvectors are needed to calculate the force on the atoms.

2.2.4 Summary and further details

The general algorithm for the numerical studies can be summarized in the following way:

1. Create an initial trial vector \vec{u} for the oxygen positions.
2. Diagonalize the corresponding Hamiltonian matrix.
3. Calculate the force \vec{F} and the matrix \hat{A} .
4. Find the new oxygen positions and build the corresponding new Hamiltonian matrix.
5. Return to 2 until the displacement vector $\Delta\vec{u}$ vanishes (i.e. $\Delta\vec{u} * \Delta\vec{u} <$ threshold)

The minimization algorithm sometimes runs into metastable solutions. Therefore, different initialization of the starting vector \vec{u} are used.

Besides the shape of the finite clusters is varied, i.e. the calculations are not restricted to cubic or orthorhombic clusters but can have more general shapes. The advantage of this freedom, although it takes some extra efforts to construct the corresponding Hamiltonian matrix, is that artificial degeneracies, which occur by choosing very symmetric cells, can be partly lifted. This enhances the quality of the numerical results and decreases empirically the chance to obtain metastable solutions. Especially very asymmetric supercells with equal length of the translation vectors are most advantageous.

Chapter 3

The Peierls insulator BaBiO_3

3.1 Introduction: 1D-metal-insulator transitions

The insulating properties of BaBiO_3 provide some challenge for theoretical explanations. Since the conduction band Bi $6s$ is half-filled, metallic behavior is expected in the independent electron picture or from simple band-theory arguments. Assuming a perfect cubic perovskite structure of the material, band structure calculations predict a half-filled broad band made of Bi $6s$ electrons anti-bonded with O $2p_\sigma$ states [13],[14], [23]. The size of the $6s$ orbital is large and thus, the single electron or band approximation should be good. However, the real crystal structure of BaBiO_3 deviates from the perfect perovskite symmetry. The oxygen-octahedra show tilting and breathing-type distortions and therefore suggest that a charge instability for the Bi-sites exists.

Theories, explaining the insulating behavior in this material, can be roughly divided, whether electron-electron correlations or electron-phonon in-

interactions are believed to be the dominant process. Both theories were first developed for the one dimensional metal and rest on the observation, that the Lindhard response function of the one dimensional electron gas $\chi(q) = \int \frac{dk}{2\pi} \frac{f_k - f_{k+q}}{\epsilon_k - \epsilon_{k+q}}$, where $f_k = f(\epsilon_k)$ is the Fermi function, diverges at $q = 2k_F$. The divergence is due to a particular topology of the Fermi surface, called perfect nesting. Pairs of states, one full and one empty, that differ by $q = 2k_F$ have the same energy and therefore, give a diverging contribution to the integral in χ . The divergence of the response function has important consequences. It implies that an external perturbation $V(r) = \int_q V(q)e^{iqr}dq$ leads to a divergent charge redistribution $\rho_{ind}(r) = \int_q \chi(q)V(q)e^{iqr}dq$. This suggests through self-consistency, that at $T = 0$ the electron gas itself is unstable with respect to the formation of a varying electron-charge or electron-spin distribution with period $\lambda = \pi/k_f$ [24].

Overhauser [25] discussed the one dimensional Hubbard model and showed that the 1D metal transforms into an insulator due to electron-electron interactions forming a spin-density wave. Although BaBiO₃ does not have a spin-density wave, Varma suggested that a negative U arising from intra-atomic interaction could exist in BBO. It is responsible for the valence-skipping of the Bi⁴⁺ and thus, accounts for a charge density wave [26]. This idea was checked by Vielsack and Weber [27], performing constrained density functional calculations in order to extract U values for BBO. Their results provide no evidence for a negative Hubbard U of purely electronic origin and are supported by the LDA calculations of Meregalli and Savrasov [28].

The other candidate, resulting in a charge density wave ground state, without the detour of a negative Hubbard U , is the coupling of the electrons to the underlying lattice. This was first demonstrated by Peierls [29]. The

electron-phonon interaction splits the energy bands at the Fermi-energy and transforms the metal into an insulator, while freezing in the phonon with $q = 2k_F$. This phonon mode is occupied macroscopically and causes a static distortion of the lattice.

In both cases, electron-electron or electron-phonon interaction, the perfect nesting property of the Fermi-surface is a prerequisite for the phase transition. The periodicity of the CDW is not necessarily pinned to lattice periodicity but is determined by the nesting vector at Fermi-energy. These nesting properties, on the other hand, are harder to obtain in multi-dimensional systems. Nearest-neighbor tight binding models [13] give perfect nesting at the Fermi energy in BaBiO₃ and more realistic models partially preserve this property. However, for the doped material the nesting degeneracy is lifted and metallic behavior is predicted. The simplified RS-model describes the charge-density wave in the half-filled case driven by nesting on a 3D Peierls scenario. It can also serve as a model for the insulating behavior under light doping (Chapter 4).

It will be important to understand the two parts of the Hamiltonian and their interplay in more depth. We therefore start in this chapter with analyzing the non-interacting Hamiltonian H_t and the interaction part $H_{e-ph} + H_{ph}$ separately, before we review the analytical solution [20] for the Rice-Sneddon model in the half-filled case. In the numerical section, the interplay between H_t and H_{e-ph} will be investigated further. Different pictures of the ground-state emerge, depending on the coupling strength Γ . The chapter closes with a section on experimental results in BaBiO₃ and an estimate for Γ in based on experiment and theory.

3.2 The extremes: $g \rightarrow 0$ and $t \rightarrow 0$

3.2.1 Delocalized electron states: $g = 0$

Neglecting the electron-phonon term ($g = 0$), the band-structure is modeled by the hopping term, describing metallic behavior of the system and yielding a simple cosine dispersion:

$$\epsilon_{\vec{k}} = -2t(\cos(k_x a) + \cos(k_y a) + \cos(k_z a)). \quad (3.1)$$

The band minimum is at $\vec{k} = 0$ and the bands are symmetric around $\epsilon_{\vec{k}} = 0$, which is the Fermi energy at half-filling. The dispersion has the symmetry property $\epsilon_{\vec{k}+\vec{Q}} = -\epsilon_{\vec{k}}$, where $\vec{Q} = (\pi/a, \pi/a, \pi/a)$. This leads to perfect nesting, when the Fermi energy is zero, because for each \vec{k} with $\epsilon_{\vec{k}} = 0$, there exists another state corresponding to $\vec{k} + \vec{Q}$, which is also at the Fermi energy.

The charge-density is distributed homogeneously over the entire crystal and the wave-functions are delocalized, i.e. the electrons are described as Bloch-waves with wave-vector \vec{k} and their effective mass given by $m_{\text{eff}}^{ij} = (\frac{1}{\hbar^2} \frac{d^2 \epsilon_{\vec{k}}}{dk_i dk_j})^{-1}$, which we define to be m_{ij}^* . The energy per atom of the system at half-filling is given by:

$$E_{\text{tot}}/N = \int_{\text{occ}} d^3k D(k) \epsilon_k = -2t \quad (3.2)$$

3.2.2 Localized electron states: $t = 0$

In the opposite limit, the RS-model describes insulating behavior at half-filling. The ground state consists of symmetric breathing type distortions of amplitude e around the Bi sites and the Bi-lattice splits into an A and B-site type. Electrons on A sites have their energy lowered by $-ge = -6gu$ and electrons

on B sites their energy raised by $ge = 6gu$. The ground state at half-filling consists of electron pairs localized on A sites and empty B-sites, i.e. the charge is completely disproportionated (see Fig.2.1). The distortion amplitude u is controlled by the elastic energy term. To find the optimal distortion amplitude u_0 , the system energy $E_{\text{tot}} = N(-6gu + 3/2Ku^2)$ has to be minimized with respect to u , leading to

$$u_0 = \frac{2g}{K}. \quad (3.3)$$

Thus, the energy density of the system, is given by:

$$E_{\text{tot}}/N = -12\frac{g^2}{K} + 6\frac{g^2}{K} = -6\frac{g^2}{K} \quad (3.4)$$

In this limit also on-site electron-electron interaction can be added without creating too much complication. The effect of the electron-phonon term can be replaced by an effective negative Hubbard U . The oxygen-ion polarization overscreens the on-site Coulomb repulsion.

3.3 Analytical studies of the CDW instability for a half-filled band

For half-filling, the electron dispersion shows strong nesting at the Fermi energy with nesting vector $\vec{Q} = \frac{\pi}{a}(1, 1, 1)$ (see Sec.(3.2.1)). Thus, for arbitrarily weak electron-phonon coupling, the homogeneous charge distribution is unstable with respect to the formation of a commensurate charge-density wave with wave-vector \vec{Q} . The system is unstable against static breathing-mode type distortion of the oxygens. Oxygens are displaced by $u(l, \alpha) = \pm \frac{e_0}{6}$ outward

(+), away from half of the Bi atoms, and inward (-), toward the other half. The dilatation alternates from cell to cell.

The ground-state of the system is therefore, characterized by an ordered oxygen-displacement wave (ODW) with wave-vector \vec{Q} and an order parameter defined as:

$$u(l, \alpha) = u_0 \exp(i\vec{Q}\vec{R}_l) = \pm u_0 \quad (3.5)$$

or

$$e(l) = e_0 \exp(i\vec{Q}\vec{R}_l) = \pm e_0, \quad (3.6)$$

plus a charge density wave (CDW) with same wave-vector \vec{Q} and amplitude ρ_0 :

$$\rho(l) = \langle c_l^\dagger c_l \rangle = 1 + \rho_0 \exp(i\vec{Q}\vec{R}_l) = 1 \pm \rho_0. \quad (3.7)$$

Thus, the unit cell of the original lattice is doubled and two distinct sublattices A and B form a rocksalt lattice, changing the translational symmetry to fcc-symmetry. Sites on the A sublattice are defined to have positive $e(l)$ and the orbitals $|l\rangle$ have their energy lowered. The B sublattice is defined correspondingly.

To see the opening of the gap in the energy spectrum, we first derive the new dispersion relation, inserting (3.5) and (3.6) in H. Then, the amplitude $e_0 = 6u_0$ and the excess charge ρ_0 have to be determined self consistently.

3.3.1 Opening of the Peierls gap

A convenient basis to work in are the Bloch functions [20]:

$$|\vec{k}A\rangle = \frac{1}{\sqrt{(N/2)}} \sum_l^{\text{Asublattice}} e^{i\vec{k}\cdot\vec{R}_l} |l\rangle \quad (3.8)$$

and the corresponding functions for the B sublattice.

In this basis set the Hamiltonian separates into 2x2 blocks:

$$H_{red} = \begin{pmatrix} -\Delta & \epsilon_{\vec{k}} \\ \epsilon_{\vec{k}} & \Delta \end{pmatrix} \quad (3.9)$$

with

$$\Delta = ge_0 = t\sqrt{\Gamma}e_0 \quad (3.10)$$

and $\epsilon_{\vec{k}}$ the eigenvalues of the undistorted problem.

Now the problem can be solved in the standard way. The energy eigenvalues are:

$$E_{\vec{k}} = \pm \sqrt{\epsilon_{\vec{k}}^2 + \Delta^2}. \quad (3.11)$$

Defining an angle $2\theta_{\vec{k}}$ by

$$\tan(2\theta_{\vec{k}}) = \frac{\epsilon_{\vec{k}}}{\Delta}, \quad (3.12)$$

the corresponding eigenvectors for positive and negative $E_{\vec{k}}$ read:

$$|\vec{k}-\rangle = \cos(\theta_{\vec{k}})|\vec{k}A\rangle + \sin(\theta_{\vec{k}})|\vec{k}B\rangle \quad (3.13)$$

$$|\vec{k}+\rangle = \sin(\theta_{\vec{k}})|\vec{k}A\rangle - \cos(\theta_{\vec{k}})|\vec{k}B\rangle. \quad (3.14)$$

The distortion of the oxygens splits the $6s$ band into two Peierls bands $\vec{k}+$ and $\vec{k}-$. These bands are separated by a minimal energy of 2Δ . All states $|\vec{k}-\rangle$ in the lower Peierls band are occupied twice due to spin degeneracy, leaving the upper band empty and thus, account for the insulating behavior of the

system. The many body wave-function for the ground state in the half-filled case, therefore reads:

$$|G \rangle = \prod_{\vec{k}, \sigma} c_{\vec{k}-}^\dagger |\text{vac} \rangle . \quad (3.15)$$

The density of states $D(E)$ can be evaluated in terms of the density D_0 of undistorted problem using $D(E)dE = D_0(\epsilon)d\epsilon$ and Eq. (3.11):

$$D(E) = D_0(\sqrt{E^2 - \Delta^2}) \frac{|E|}{\sqrt{E^2 - \Delta^2}} \theta(|E| - \Delta) \quad (3.16)$$

$D(E)$ has an inverse square root singularity at the band edge and is shown in Fig.3.1.

Further analysis of the dispersion and the eigenvectors shows, that mainly the states at the top of the valence band are responsible for the charge separation. The splitting of the original lattice in A and B sublattice doubles the unit cell and therefore reduces the Brillouin zone. In the reduced part of the Brillouin zone (RBZ), the eigenvalues $\epsilon_{\vec{k}}$ and thus, $\theta_{\vec{k}}$ are negative for nearly all \vec{k} . Therefore, the lower Peierls band is mainly built from states which are bonding, i.e. in phase between A and B sites. On the other hand, for states at the band edge ($\epsilon_{\vec{k}} = 0 \rightarrow \tan(2\theta_{\vec{k}}) = 0$) the amplitude vanishes on B sites for valence band states and on A sites for conduction band states. This means, mainly the states at the top of the valence band, which are also highest in density, are responsible for the charge disproportion.

From the new dispersion relation Eq. (3.11), we see furthermore, that the effective mass of the electrons gets enhanced with respect to the non-interacting mass m_{ij}^* . For strong coupling the leading term in the effective mass is proportional to the ratio of the gap Δ to the non-interacting band

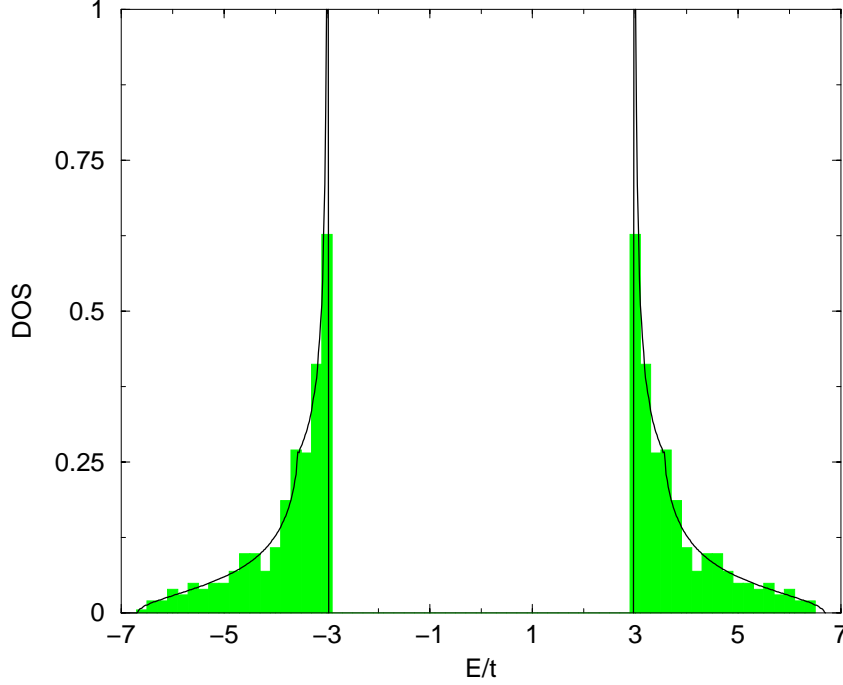


Figure 3.1: Density of states for $\Gamma = 0.3$, evaluated with a tetrahedron code [30][31] (line) together with a histogram obtained by diagonalizing H for a super-cell with 1020 Bi atoms

energy $\epsilon_{\vec{k}}$:

$$m_{\text{eff}}^{ij} \sim \frac{\Delta}{\epsilon_{\vec{k}}} m_{ij}^* \quad (3.17)$$

3.3.2 Self-consistent determination of the ODW- and CDW-amplitudes

Gap and ODW-amplitude

In order to determine the optimum distortion amplitude u_0 or $\Delta = 6t\sqrt{\Gamma}u_0$ respectively, one has to minimize the total energy of the system, which is given

by the sum $E_{\vec{k}}$ over all occupied states E_e plus the elastic energy E_L :

$$E_{\text{tot}} = E_e + E_L = -2 \sum_{\vec{k}}^{\text{RBZ}} \sqrt{\Delta(u_0)^2 + \epsilon_{\vec{k}}^2} + \frac{3NKu_0^2}{2} \quad (3.18)$$

Minimizing this with respect to u_0 yields an equation for the gap, which reads after inserting the expression Eq. (2.10) for the dimensionless coupling constant :

$$\frac{1}{12\Gamma} = \frac{2}{N} \sum_k^{\text{RBZ}} \frac{1}{\sqrt{(\epsilon_{\vec{k}}/t)^2 + (\Delta/t)^2}} \quad (3.19)$$

The gap-equation Eq. (3.19) can be approximated for weak and strong coupling. For small Γ one obtains the familiar BCS exponential law [20]:

$$\frac{\Delta}{t} = C_1 \exp(-1/C_2\Gamma) \text{ for } \Gamma \ll 1 \quad (3.20)$$

with $C_1 = 6.5$ and $C_2 = 3.44$.

For strong coupling the gap behaves almost linear in Γ [20]:

$$\frac{\Delta}{t} = 12\Gamma \left(1 - \frac{1}{48\Gamma^2}\right) \quad (3.21)$$

and approaches asymptotically the value obtained for $t = 0$:

$$\Delta = 12 \frac{g^2}{K} \rightarrow \frac{\Delta}{t} = 12\Gamma. \quad (3.22)$$

The amplitude of the ODW u_0 is directly related to Δ by $\Delta = 6gu_0$.

CDW-amplitude

What is left is to find an expression for the amplitude ρ_0 of the CDW.

Making use of the inverse relation of (3.13) and (3.14):

$$|\vec{k}A\rangle = \sin(\theta_{\vec{k}})|\vec{k}+\rangle + \cos(\theta_{\vec{k}})|\vec{k}-\rangle \quad (3.23)$$

and the fact that for the half filled case the upper band is empty, the expectation value $\langle c_l^\dagger c_l \rangle$ determining ρ_0 can be evaluated the following way:

$$\rho_A = 1 + \rho_0 = 2\langle c_l^\dagger c_l \rangle_A = \frac{4}{N} \sum_{\vec{k}}^{RBZ} \langle c_{\vec{k}A}^\dagger c_{\vec{k}A} \rangle = \frac{4}{N} \sum_{\vec{k}}^{RBZ} \cos^2(\theta_{\vec{k}}) \quad (3.24)$$

Taking the value $\cos \theta_{\vec{k}}$ from (3.12) and using the gap-equation (3.19) one finally arrives at:

$$\rho_0 = \frac{\Delta/t}{12\Gamma}. \quad (3.25)$$

3.3.3 Artifacts of the model

Some results are special properties of the simplified Rice-Sneddon Hamiltonian. The perfect nesting property at the Fermi energy at half filling is destroyed by adding further range hopping. Thus, the charge-density wave instability is inhibited. Nevertheless, a charge-ordered state is still the ground state, when the electron-lattice coupling exceeds a critical value. The perfect nesting property, therefore, is not required for a charge separated ground state and we will introduce in the next chapter the concept of a "bipolaronic crystal", to clarify this point.

Adding a not too large Hubbard U to the Hamiltonian also inhibits the insulating behavior and a threshold distortion exists before the lower and upper Peierls band get separated by a gap [19]. Since the electron-phonon term is the source of a negative, i.e. attractive U , it is clear, that the coupling has to exceed a certain strength to overscreen the repelling electronic contribution to U .

3.4 Numerical results

3.4.1 Notes on the numerical calculations

Most of the numerical studies were done with an asymmetric supercell containing 210 Bi atoms. This size is sufficient regarding finite size errors for $\Gamma > 0.3$. For smaller Γ the size has to be steadily increased as Γ decreases. For $\Gamma < 0.1$ exact diagonalization results require supercells containing more than 1000 atoms and a general tendency to underestimate the gap compared to the results obtained with the tetrahedron code is observed. The starting conditions for the oxygen-distortion vector \vec{u} were varied. In general, the program could find the minimum easily, when the ODW-behavior was initialized with arbitrary amplitude.

3.4.2 Hopping versus electron-phonon-term: competition and compromise in the half-filled case

The analysis of the separate contributions to the Hamiltonian at half filling in Sec.(3.2) showed that hopping and the electron-phonon term have opposite preferences in terms of localization of the charge density. It is therefore natural to expect some competition of the two terms, when they act simultaneously in a system. On the other hand, it is a quantum mechanical rule, that starting off with one term in the Hamiltonian, adding a second one will lower the energy of the system. Therefore, hopping and electron-phonon terms will try to find a compromise. The particular compromise will certainly depend on which of the two terms is dominant in terms of lowering the total energy.

Charge-density wave concept for weak electron-phonon coupling

If hopping is the dominant process, the electron-phonon term can be treated perturbatively. In this case the behavior of the system is determined by the band-structure and the particular topology at the Fermi surface. If there is no nesting at the Fermi-energy, the effect of weak electron-phonon coupling results in a mass renormalization of the band mass but the metallic property will be preserved. On the other hand, perfect nesting at the Fermi energy causes an instability of the metallic state against infinitesimal perturbations with periodicity of the nesting vector. The electron-phonon term creates a charge-density and static lattice displacement wave, opening a gap at the Fermi-energy, and transforms the metal into an insulator. Thus, the effect of the electron-phonon term is tremendous in this case as it causes a phase transition of the material. However, the effect in the energy is small and can be handled perturbatively once the symmetry breaking is treated self-consistently. Signature of this state, is a weak spatial oscillation of the charge density increasing exponentially with $-1/\Gamma$. The hopping term still dominates the total energy and effective mass of the band electrons.

Bipolaronic crystal concept for strong electron-phonon coupling

Contrary to the CDW-formation, the charge-ordered ground state is more or less independent of the particular topology of the Fermi-surface, if the electron-phonon term is strong enough. Electrons pair on Bi^{3+} sites and cause a strong response of the oxygens forming Bi^{5+}O_6 molecules. In this case, it is more appropriate, to characterize the ground-state as a bipolaronic crystal and reserve the term “charge density wave” for a charge-ordered state caused

by a nesting instability of the electron system. Electrons or holes have strong localization properties caused by the strong lattice response on Bi^{3+} and Bi^{5+} sites, respectively. The term bipolaron will be explained in more detail in the next chapter.

Now hopping acts perturbatively and electrons are allowed to delocalize. As a result, the ideal charge disproportion in Bi^{3+} and Bi^{5+} will become incomplete and the wave-function become Bloch-waves. However, the effective mass is dominated by Δ and can be multiples of the band mass. Thus, since coherent band motion of “heavy” charge carriers can be destroyed more easily, the localized aspects of the electrons become more important.

Competition and compromise

The competition of the two terms is probably most clearly reflected in the development of the system energy with Γ . In Fig.(3.2) the total energy per atom $E_{\text{tot}} = E_e + E_L$ and its contributions the electronic part E_e and the elastic energy contribution E_L are displayed separately. If hopping dominates, we expect a weak charge disproportion. If the electron-phonon term is dominant, an almost complete charge disproportion is anticipated. The opposite nature of the two terms yields a rather quick transition from one to the other.

The electronic part of the energy per atom E_e shows indeed a sharp crossover from the pure hopping limit $E_e^{g=0} = -2t$ to the pure electron-phonon interaction limit $E_e^{t=0} = -12\frac{q^2}{K}$. The crossover occurs between $0.1 < \Gamma < 0.3$, where $\Gamma_{c1} = \frac{1}{6} \approx 0.167$ marks the coupling strength, when $E_e^{t=0} = E_e^{g=0}$ and the deviation from either limit is biggest. E_L has a kink, too in this interval and also the excess charge ρ_0 increases rapidly, there (see Fig.3.3). However, the excess charge still differs from 1 for $\Gamma > 0.3$ and approaches

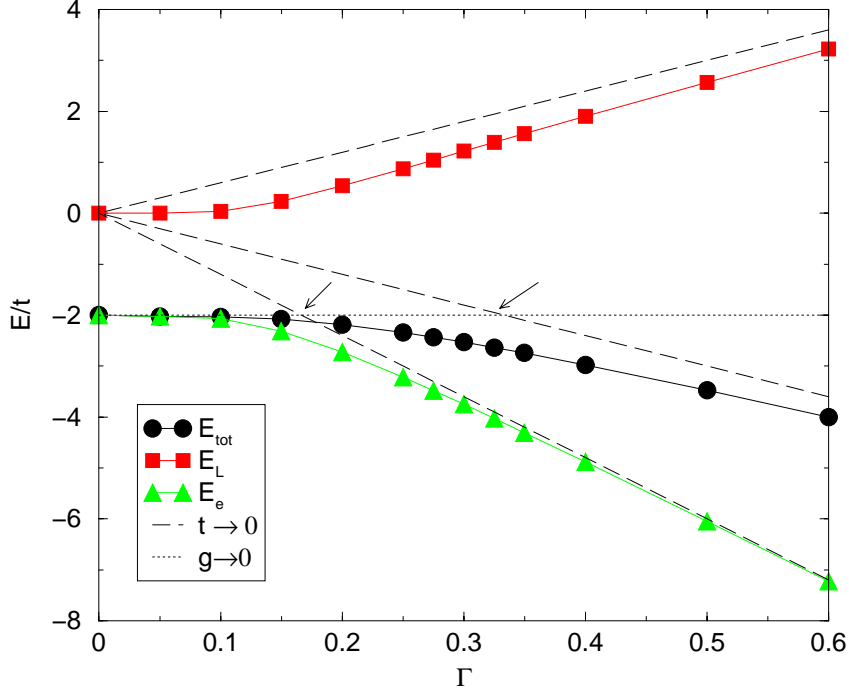


Figure 3.2: Γ -dependence of the system energy per atom E_{tot} , E_L and E_e , arrows indicate Γ_{c1} and Γ_{c2}

the complete charge separated state rather slowly. This is the effect of the hopping term. The incomplete charge disproportion is the way of compromising hopping and electron-phonon term and leads to a smaller u_0 or gap 2Δ (see Eq.(3.10),(3.25)). In turn, the elastic energy costs E_L are reduced and converge rather slowly against the $t = 0$ limit. As a result, the total energy E_{tot} is lowered and approaches the asymptotic value very slowly. The development of E_{tot} is rather smooth and exhibits no clear kink, contrary to E_L and E_e . This is because the changes in E_L and E_e partly compensate each other. The states accounting for the incomplete charge-disproportion are those at the

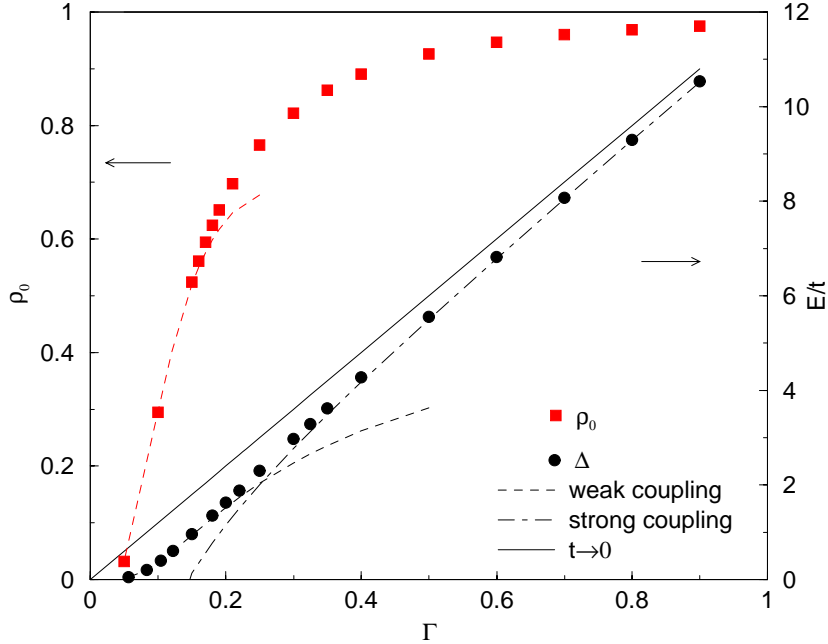


Figure 3.3: Γ -dependence of Δ and the CDW-amplitude ρ_0

bottom of the lower Peierls band, which profit most from hopping and thus have delocalized character. As stated previously, towards the top of the band states localize increasingly more easily.

Since E_{tot} is the physically relevant number, a second critical coupling constant Γ_{c2} can be assigned. For $\Gamma_{c2} = \frac{1}{3}$ the energy of pure hopping $E_{tot} = -2t$ and pure interaction $E_{tot} = -6\frac{g^2}{K}$ (see Sec.3.2.1 and Sec.3.2.2) are equal and the difference of the actual energy and the the two limits $t = 0$ and $g = 0$ is biggest. Thus, Γ_{c2} denotes the coupling strength, where the transition between hopping as dominant and electron-phonon as dominant process should definitely occur. Based on the results for E_e and E_L , it seems reasonable to suppose that the transition starts earlier and the most significant

changes in the system happen in the range between 0.1 and Γ_{c2} . This is further supported by the behavior of the gap. The weak coupling formula Eq.(3.20) agrees nicely with the numerical values for $\Gamma \leq 0.2$ and the strong coupling formula Eq.(3.21) starts to work reasonably well for $\Gamma \geq \Gamma_{c2}$ (relative deviation at $\Gamma = 0.325$ is 5% and at $\Gamma = 0.9$ only 0.1%).

Conclusion

The simplified RS-model exhibits a charge-ordered ground state at half filling. For small Γ , hopping is the dominant factor and nesting properties at the Fermi energy are decisive to transform the metal into an insulator. The charge ordered state can be described in terms of a commensurate charge density wave. For strong coupling the electron-phonon term dominates and the idea of a bipolaronic crystal or local-CDW describes the behavior of the system more accurately. Details of the band structure are less important in this limit. The transition between the two extremes occurs in the range between $0.1 < \Gamma < 0.33$.

3.5 Experiment and theory

3.5.1 Experimental results

The conclusion that BaBiO₃ exhibits a charge-ordered ground-state, comes from structural investigations. Neutron diffraction experiments identify superlattice peaks, that indicate symmetric breathing-type oxygen distortions besides tilting distortions [6], [32]-[35]. The Bi-O bond lengths have been

refined to be e.g. in Ref. [35] $\text{Bi}(1)\text{-O} = 2.11\text{\AA}$, $\text{Bi}(2)\text{-O} = 2.29\text{\AA}$, which corresponds to $u_0 = 0.09\text{\AA}$. This is smaller than what is expected from a complete charge disproportion (Shannon radii: $\text{Bi-O}^{3+} = 2.11\text{\AA}$, $\text{Bi-O}^{5+} = 2.38\text{\AA}$). The effective valences for the Bi atoms have been assigned according to Rietveld refinements varying between +3.9 to +3.5 and +4 to +4.4 [34]. Also photoemission experiments find a weak feature that might indicate different Bi-types (but could also be explained in other ways) [36]-[38].

Various optical experiments measure an optical gap of about 2eV, that can be associated with excitations across the Peierls gap 2Δ [39]-[41].

3.5.2 Determination of Γ and comparison between theory and experiment

The simplified RS-model relates the gap 2Δ to the value of the static oxygen displacement u_0 and to ρ_0 . To compare experiment with the theory, the parameters t , K and g have to be determined.

The effective hopping integral t between the Bi sites is chosen, that the bandwidth of the valence-band $W \approx 4.1\text{eV}$, coming from band-structure calculations for the cubic phase [42] [28], agrees with the width of the cosine dispersion band $W = 12t$. This yields $t = 0.34\text{eV}$.

From the optical data, we take $2\Delta = 2\text{eV}$ and obtain, together with the estimate for $t = 0.34\text{ eV}$, the value for $\frac{\Delta}{t} \approx 3$.

Therefore, Γ can be extracted from Fig:(3.3) to be:

$$\Gamma \approx 0.3. \tag{3.26}$$

ω_0 is determined by Raman experiments, where a breathing mode with energy 570cm^{-1} (70meV) is identified [43]. Together with the oxygen mass $M = 16u$

this yields a elastic constant $K = 19\text{eV}/\text{\AA}^2$. Finally g is calculated from $\Gamma = \frac{g^2}{Kt}$, giving $g = 1.4\text{eV}/\text{\AA}$.

Parameter	Value
t	0.34eV
K	19 eV/ \AA^2
g	1.4 eV/ \AA
Γ	0.3

With these values u_0 is predicted to be $u_0 = \frac{\Delta}{6g} = 0.12\text{\AA}$, which compares to the experimental value of 0.09\AA . The theoretical value $\rho_0 \approx 0.8$ is also overestimated by the RS-model. It should be mentioned, that the refined Γ value 0.3 lies in the transition area between a hopping and electron-phonon dominated system, where ρ_0 and u_0 are very sensitive to small changes in Γ . However, $\Gamma = 0.3$ lies closer to the limit of a clearly phonon-dominated system. The spatial dimension of the electron-electron pairs can be estimated by $\xi = \frac{\hbar v_F}{\pi\Delta}$ [24]. Tajima [44] estimated $\xi = 3\text{\AA}$ for BaBiO_3 . This is less than the spacing between two adjacent Bi-atoms and supports a more local view of the system in terms of the bipolaronic crystal picture. A weak quasi one-dimensional CDW-system is $\text{K}_{0.3}\text{MoO}_3$. Here Δ is only 0.07 eV and ξ is estimated to be $\xi = 29\text{\AA}$ [24]. We expect therefore that the physics in BaBiO_3 can be understood starting from the bipolaronic crystal limit.

Chapter 4

Light doping of the charge-ordered state: polaron and bipolaron formation

4.1 Introduction

4.1.1 Theories for the MI-transition under doping

The real theoretical challenge, when studying the normal state properties of the BBO system, is the metal to insulator transition under doping. In the $\text{Ba}_{1-x}\text{K}_x\text{BiO}_3$ alloys the semi-conducting properties persist up to an unusual high doping concentration of $x = 0.35$, when hole-doped with Pb up to $x = 0.65$. Since the Pb atoms replace the Bi atoms, doping the band-filling also and nature of the conduction band. Potassium on the other hand replaces the passive Ba-atoms and has a negligible effect on the Bi-O bands [13]. Thus, intrinsic effects associated with band-filling can be studied in the K-doped

compounds.

If Coulomb interaction between the charge carriers is again omitted, there are still various schemes, that could explain the persistence of insulating behavior in the presence of dopants. Starting from the picture of a weak-coupling commensurate CDW-formation on a Peierls-nesting scenario for the undoped system, the formation of incommensurate charge density waves in the doped materials has been proposed. As already mentioned, sufficient nesting that causes a charge instability away from half-filling are harder to obtain in three dimensional systems than in 1D. However, the process could be assisted by chemical ordering of the dopants in the supercell, i.e. the K ions adopt helpful positions to maintain the CDW [45] [46].

More recent, phase separation or stripe formation has been suggested, to explain the insulating behavior. The doped holes collect in hole rich regions and spatially separate from undoped insulating phases. The doped regions may or may not become metallic. This process could also be assisted by chemical ordering waves of the counter ions.

Another route to the MI transition follows the idea of strong electron-lattice interaction. One could expect some mechanism that immobilizes the charge carriers due to electron-phonon interaction. This process is commonly known under the term “self-trapped or small polaron formation”. Yu et al. studied a 2D-Rice-Sneddon model along these lines for a large dopant concentration [21]. For the lightly doped material a variational calculation has been performed by Allen and Kostur [20] in order to estimate the critical coupling constant that permits such a scenario to happen.

In this chapter, we perform detailed numerical calculation for the dilute doped

material on the stability and nature of polarons and bipolarons with respect to the coupling constant Γ . We first introduce the general concept of “self-trapped polarons” and review some results of similar studies for the empty band Rice-Sneddon model [47]. The numerical section studies the stability of (bi)polaron formation and several many-body and single particle properties of the solutions. In the last section, we compare the results to the empty band case and give a brief overview over related experiments.

4.1.2 General introduction to polaron theory

The quasi-particle composed of an electron or hole and the pattern of lattice displacement is called a polaron. The idea was first introduced by Landau as an attempt to explain the optical properties of alkali halides by the notion of exciting self-trapped carriers, i.e. exciting otherwise free carriers which become trapped or bound within potential wells produced by the displacement of atoms from their carrier-free equilibrium positions [48].

The discussion of polaron formation has ever since been performed along two lines, depending on whether long or short range interaction with phonons was studied. A continuum model for long range interaction with optical phonons was proposed by Fröhlich: it studies the charge carrier’s energy dependence on the positions of the solid’s ions through Coulomb interaction [49]. In this model, the electronic energy is lowered for arbitrarily weak values of the coupling constant α between electrons and phonons. These bound states are denoted as “large” polarons as lattice deformations extend over several unit cells, with their spatial extent continuously shrinking with increasing coupling strength. Self-trapping, in the sense of a strongly immobilized charge carrier,

in this model, however, requires unrealistic big coupling constants and for any reasonable value of α the carrier remains delocalized, with atoms responding dynamically rather than statically to the electronic motion. Thus, for weak and intermediate coupling the situation can be described by an almost free charge carrier, dressed with phonons increasing its effective mass. A large polaron generally moves coherently. The effective mass is gradually increasing with α and the weak and intermediate coupling mass renormalization results are given by [50]:

$$\frac{m^*}{m} = 1 + \frac{\alpha}{6}. \quad (4.1)$$

This model has to be contrasted to models studying situations in which the charge carrier is subject to a short range potential mediated either by acoustic phonons [53] or optical phonons [54]. They exhibit the formation of so called small polarons, that self-trap. For dimensions $d > 2$, the coupling strength has to overcome a critical value until these bound states occur. The small polaron is confined to the close neighborhood of one unit cell with displacements being a substantial fraction of the lattice constant. Its effective mass changes discontinuously at critical coupling constant and the band width becomes extremely small. The coherent motion of small polarons occurs as the self-trapped carriers follow the atoms as they tunnel from the equilibrium positions associated with the carrier occupancy of one site to those associated with carrier occupation of the other site [54]. Since the band-width is so small, the coherent motion can be readily destroyed by impurities, trapping the carrier on one ion. Thus, self-trapped small polarons move primarily incoherently through thermally assisted hopping [51] [52].

The mechanism of self-trapping has been extensively discussed by Toyozawa,

Rashba and others [53][55][56]. They studied a single charge carrier in a deformation type potential in adiabatic approximation:

$$H = \sum_{\langle i,j \rangle} t_{ij} c_i c_j^\dagger - g \sum_i Q_i c_i c_i^\dagger + \frac{K}{2} Q_i^2 \quad (4.2)$$

where the Q_i are atomic positions in configuration space.

Self-trapping is understood as a strong competition between the two processes of localization and delocalization of the charge carrier. In the presence of transfer and absence of lattice distortion the electron moves freely and the maximum energy released when the electron is allowed to extend throughout the crystal is half the bandwidth $W/2 = \nu t$ where ν is the number of next neighbors. On the other hand, neglecting hopping, the energy released by localizing the electron on one site is given by the lattice relaxation energy $E_{LR} = \frac{g^2}{2K}$.

Thus, the criterion for self-trapping reads:

$$E_{LR} > W/2 \quad (4.3)$$

Below the critical coupling constant the self-trapped state still is metastable within in a certain range. The free state, however, is always either a stable or metastable state.

4.1.3 The RS-model: self-trapping in the empty band case

The electron-phonon term in the Rice-Sneddon-model is a short-range interaction term and thus, the Toyozawa model and the RS-model are similar. In fact, a study on polarons in the empty band case in a RS model revealed essentially the same behavior for inserted electrons in the empty band as the

Toyozawa model [47].

Below a critical coupling constant of $\Gamma = 1.96$, where Γ is defined according to Eq.(2.10), the system is stable against lattice distortions and the wave function remains delocalized. Non-adiabatic coupling with virtual phonons leads to a self energy shift of $\approx 0.09\Gamma t$ and suggests a comparison to the large Fröhlich polaron. A unique translation between this two pictures, however, cannot be given [47].

Above Γ_c a small self-trapped polaron with an initial localization of 90 % of the electron density on one ion is formed, the typical distortions are $u \approx 0.03a$ and decay exponentially far from the center of the polaron. A gap Δ_p opens in the electron spectrum- separating the lower lying localized state from the delocalized band states. Besides, a region of metastability for small polarons is found numerically and confirmed by variational calculations [47].

A comparison with the Toyozawa model shows that Γ_c can be estimated from the localization-delocalization criterion. The optimal distortion for an electron localized on one ion when hopping is neglected, is given by $u = \frac{g}{k}$, leading to a lattice relaxation energy of $E_{LR} = 3\frac{g^2}{K}$. This has to be compared to the half band-width $W/2 = 6t$.

Thus:

$$3\frac{g^2}{K} > 6t \rightarrow \Gamma = \frac{g^2}{Kt} > 2. \quad (4.4)$$

Therefore, the process of self-trapping in the empty band case in the Rice-Sneddon model can to a good degree be understood in the terms of the Toyozawa treatment. The idea of competition between localizing and delocalization terms in the Rice-Sneddon model was already introduced in the previous chapter, when analyzing the nature of the charge ordered state. However, due

to the presence of not just one but many electrons in the system, the ability to compromise the two terms is enhanced. This will be also reflected in the case of polaron formation on the background of a charge-ordered ground-state.

4.2 The idea of self-trapping on the background of the charge-ordered state

Self-trapping of charge carriers is a process that requires a strong lattice response and domination of localizing terms over delocalizing terms. Therefore, a first reasonable step to analyze self-trapping in the charge ordered state is to completely ignore the hopping term, i.e. $t = 0$.

4.2.1 Polaron formation in the $t = 0$ case

Removing one electron from an A site, and keeping the Peierls distortion fixed, costs the amount of the attractive on-site energy $\Delta = 6gu_0 = 12\frac{g^2}{K}$ and transforms a Bi^{3+} nominally into a Bi^{4+} . However, the inserted hole reduces by one the charge difference between the site where the hole is localized and its six next neighbor Bi^{5+} -sites. Thus, the six oxygens surrounding the Bi^{4+} , experience a smaller repulsive force, and consequently relax partially to their new equilibrium positions:

$$u_0 = \frac{2g}{k} \longrightarrow u_1 = \frac{u_0}{2} = \frac{g}{k}. \quad (4.5)$$

This relaxation has a twofold effect. On the one hand, it reduces the elastic energy costs by:

$$\Delta E_L = 6\frac{K}{2}(u_1^2 - u_0^2) = -9\frac{g^2}{K}. \quad (4.6)$$

On the other hand, the relaxation changes the amount of attractive on-site energy on the Bi^{4+} site from $-6gu_0 = -12\frac{g^2}{K}$ to $-6gu_1 = -6\frac{g^2}{K}$ and pushes the energy of the half-occupied Bi^{4+} state into the gap. The difference in E_e between the ground state (two electrons occupying the state with energy $-6gu_0$) and the self-trapped state (one electron missing and the remaining electron occupying the gap state) is given by:

$$\Delta E_e = -6gu_1 - 2 * (-6gu_0) = 18\frac{g^2}{K}. \quad (4.7)$$

Thus, the creation of a self-trapped polaron costs energy E_p :

$$E_p = \Delta E_e + \Delta E_L = 9\frac{g^2}{K}. \quad (4.8)$$

Compared to the energy costs of inserting the hole without lattice relaxation, the self-trapped polaron is bound by the polaron binding energy B_p :

$$B_p = \Delta - E_p = 3\frac{g^2}{K}. \quad (4.9)$$

4.2.2 Bipolaron formation in the $t = 0$ case

Besides polarons, in order to develop a realistic model for light doping, one has to consider the possibility that the oxygen deformation overscreens the Coulomb repulsion between two holes and thus attract a second hole onto the same site. In other words, one has to take the possibility of bipolaron formation into account.

A bipolaron in the $t = 0$ limit corresponds to the removal of two electrons from one site and a conversion of a Bi^{3+} into a Bi^{5+} . Thus, there is no charge difference between the Bi^{5+} site and its next neighbors and therefore the surrounding oxygens relax completely, releasing elastic energy ΔE_L :

$$\Delta E_L = -6\frac{K}{2}u_0^2 = -12\frac{g^2}{K}. \quad (4.10)$$

Therefore, the creation of a bipolaron costs energy:

$$E_b = \Delta E_e + \Delta E_L = 2\Delta - 12\frac{g^2}{K} = 12\frac{g^2}{K}. \quad (4.11)$$

$-\Delta E_L$ is the net energy gain obtained by the lattice relaxation or the lattice relaxation energy $\epsilon_b = 12\frac{g^2}{K}$. In order to obtain the binding energy B_b of the bipolaron, this energy has to be compared to the binding energy of two separated, non-interacting polarons:

$$B_b = \epsilon_b - 2B_p = 6\frac{g^2}{K}. \quad (4.12)$$

4.2.3 The effect of hopping $t \neq 0$

Including the hopping term makes the problem interesting and more complicated. The vacuum of this problem is the half-filled ground-state. Including hopping we therefore change the vacuum according to the previous chapter, i.e. the oxygen distortion u_0 and the gap do not follow the simple Γ -dependence anymore.

Moreover, the inserted hole has now two competing possibilities. It can either self-localize as described in the previous subsections, or it can delocalize. The optimal delocalized states for the hole are the states at the top of the lower Peierls band, which have energy $-\Delta$. These states, however, have vanishing amplitude on B sites (see Sect.3.3.1), which means, that the hole will not spread out homogeneously over the entire crystal but reduce the average charge difference between A and B sites. This will in turn lead to a response of the oxygen atoms and therefore renormalize the gap 2Δ . In principle one could imagine that these self-consistent changes could lead to the formation of an incommensurate charge density wave. Under moderate doping the periodic

lattice should "pin" the periodicity of the Peierls distortion and doping will primarily lead to a weakening of the charge density wave and reduction of the gap.

Also, contrary to self-trapping in either the empty band or $t = 0$ case, the oxygen response to the localization process will influence the other band electrons, which cause again the oxygens to move.

All these changes have to be treated self-consistently and a simple perturbative approach is usually not working. We have not found a better treatment than numerical studies of finite systems.

4.3 Numerical results

4.3.1 Notes on the numerical calculations

For the numerical studies of polaron and bipolaron formation the algorithm described in Sec.(2.2) was used. The oxygen positions were varied until the total energy was minimized under the condition that the lowest $N/2 - 1$ energy levels were filled and the next highest was occupied singly (polaron) or left empty (bipolaron). The positions for the oxygens were usually initialized according to the Peierls order parameter. For weak coupling, the initializing was changed to the distortion pattern obtained for a self-trapped solution in a previous run, with a bigger coupling constant.

A cluster size of about 200-400 atoms was sufficient to obtain reliable values for the energy differences between the ground-state and the trapped-states. The size was increased up to 1000 atoms. For weak coupling, we took the gap values obtained by integrating the gap equation with a tetrahedron

code, to calculate the trapping energy, instead of identifying the gap with the numerical eigenvalue.

4.3.2 Stability of self-trapped states

Stability criterion

The self-trapped states compete against delocalized states and one expects a critical coupling constant Γ_c , when localized states become unstable. There are two possibilities how the transition between localized and delocalized states could occur with Γ . On the one hand, they could be separated by a potential barrier, like in the empty band case [47]. In this case a range of metastability is expected. On the other hand, they could evolve continuously, similar to a second order phase transition.

The aim of this section, is to study the transition numerically and quantify Γ_c for the insertion of one (two) hole(s) into the crystal. The delocalized state with the lowest energy is obtained, when the hole occupies a state at the top of the lower Peierls band with energy Δ . Since the force on the oxygens for delocalized holes is a n/N -effect, where n is the number of holes and N the number of Bi atoms, the effect of oxygen-relaxation can be neglected for one hole. The relative stability between delocalized and localized state is therefore evaluated with respect to Δ .

Definitions

Although the terms, formation energy E , relaxation energy ϵ and binding energy B , were already used in Sec.(4.2) we want to put them on a more formal basis according to the stability criterion.

The minimum energy required to insert a hole is denoted as polaron formation energy E_p . E_p can be expressed as the difference of the minimum energy required to insert a hole Δ without allowing lattice relaxation and the net effect of lattice relaxation given by ϵ_p :

$$E_p = \Delta - \epsilon_p. \quad (4.13)$$

ϵ_p is called lattice relaxation energy and is defined as the energy difference between the polaron state and the minimum energy of an added hole if no oxygen-displacements are permitted:

$$\epsilon_p = \langle \Psi_{\{u\}} | H | \Psi_{\{u\}} \rangle - [\langle V_{\{u_0\}} | H | V_{\{u_0\}} \rangle + \Delta] \quad (4.14)$$

where $|V_{\{u_0\}}\rangle = \prod_{k,\sigma} c_{k-}^\dagger |\text{vac}\rangle$ is the many-body wave function of the new vacuum state, the half filled band with optimum ordered displacements u_0 , and $|\Psi_{\{u\}}\rangle$ has an extra hole present and its displacements reoptimized. The bipolaron formation energy $E_b = 2\Delta - \epsilon_b$ and ϵ_b are defined analogously. Therefore, the binding energy B_p equals the relaxation energy in the polaron case:

$$B_p = \epsilon_p. \quad (4.15)$$

No Coulomb repulsion between the holes is included in our model. Thus, the bipolaron binding energy B_b is given by the difference of ϵ_b and the binding energy of two separated, non interacting polarons $2\epsilon_p$.

$$B_b = 2\epsilon_p - \epsilon_b. \quad (4.16)$$

Polaron formation

Localized bound polaron states were obtained numerically for $\Gamma_c^p > 0.18$. Below the critical coupling constant only delocalized states were found. Close to

the critical coupling constant, the polaron binding energy is very small and one can speculate, that it might be a metastable state compared to a delocalized state. No range of metastability is found numerically. The delocalized numerical solutions at Γ_c^p , were comparable in energy, but unstable with respect to small distortions toward a polaron state. Our results are compatible with a continuous evolution of the polaron state similar to a second order transition with Γ . This contrasts with the empty band case, where a first-order instability was found [47].

The Γ -dependence of the lattice relaxation energy for the polaron in the physically interesting range between $0 < \Gamma < 1$ is shown in Fig.(4.1). ϵ_p approaches asymptotically the $t = 0$ limit $\epsilon_p = 3\Gamma t$, but the deviations are considerable in this range. The problems related to find easy perturbative formulas were already mentioned in Sec.(4.2.3). The vacuum changes with t and screening effects of other band electrons have to be taken into account self-consistently. Phenomenologically a better “fit” to ϵ_p can be obtained by approximating ϵ_p , according to:

$$\epsilon_p/t \approx \Delta(\Gamma) - 9\Gamma \rightarrow 3\Gamma - \frac{1}{4\Gamma}. \quad (4.17)$$

This fit is based on the observation that in the equation $\epsilon_p = \Delta - E_p$, the nonlinear contributions to E_p are weaker than to Δ and corresponds formally to the introduction of the strong coupling values for u_0 into Eq.(4.5)-Eq.(4.9), i.e. it corresponds to a vacuum correction of the trapping energy.

Let us illustrate the failure of a simple perturbative approach, by analyzing the nonlinear corrections to E_p . E_p can be decomposed in the changes caused by the lattice response to the presence of the hole ΔE_L and the changes of the

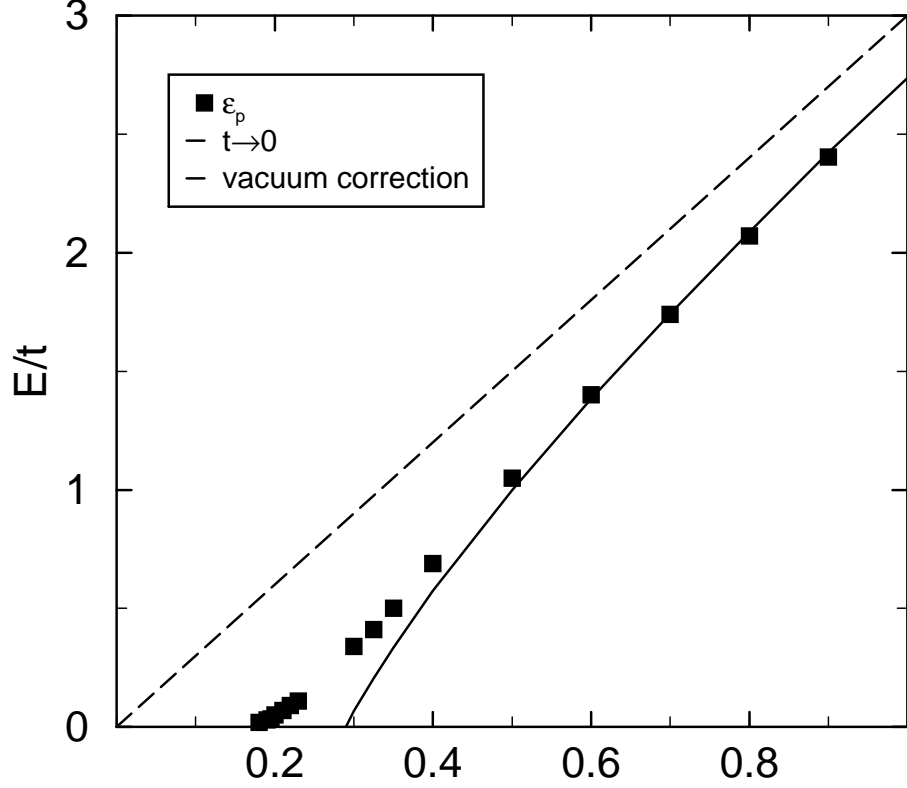


Figure 4.1: Polaron lattice relaxation energy ϵ_p

electronic energy ΔE_e compared to corresponding vacuum. In a perturbative approach deviations in both, the vacuum and the final state, have to be taken into account. In the final state the localized hole starts to delocalize. This will lower the energy $\epsilon_s/t = -6\Gamma$ of the gap state (see Sec.(4.3.3)), which is occupied with one electron, by a term c/Γ . Therefore, if we neglect changes in the states of the other electrons, one predicts that the true ΔE_e should be smaller than in the $t = 0$ limit, since analogously to Sec.(4.2.1):

$$\Delta E_e/t = 1/t[\Delta + (\epsilon_s + \Delta)] = 18\Gamma - \left(\frac{1}{2} + c\right)\frac{1}{\Gamma}, \quad (4.18)$$

where we included the change in the vacuum, using the strong coupling formula for Δ . Similarly, one expects an increase of $\Delta E_L/t$ compared to the $t = 0$ limit, if only the response u_1 of the six oxygens surrounding the polaron is taken into account. If we simply include the vacuum correction and leave $u_1 = g/K$, we obtain:

$$\Delta E_L/t = 3K/t(u_1^2 - u_0^2) = -9\Gamma + \frac{1}{2\Gamma} - O(1/\Gamma^3). \quad (4.19)$$

Certainly u_1 deviates from the $t = 0$ limit, too, when the polaron wave-function extends to the neighboring sites. To change the sign of the $1/\Gamma$ correction in Eq.(4.19) this correction would have to exceed $\frac{1}{2\Gamma}$.

The numerical results of ΔE_e and ΔE_L for $\Gamma < 1$ show the opposite behavior from what is expected from these simple strong coupling arguments. ΔE_e is increasing with Γ and ΔE_L is decreasing. This indicates that the changes caused by the presence of the other electrons have to be taken into account self-consistently in the perturbation expansion. The linear behavior of E_p is due to effect that the nonlinear contributions in ΔE_e and ΔE_L almost cancel each other, down to $\Gamma \approx 0.35$.

Bipolaron formation

The numerical onset for bipolaron stability against two delocalized holes was found to be $\Gamma_c^b = 0.15$, a little smaller than for the polaron state ($\Gamma_c^p = 0.18$). If Coulomb repulsion is neglected, two spatially separated polarons are always unstable with respect to the creation of a bipolaron state, where both holes sit on the same site. The bipolaron relaxation energy ϵ_b approaches asymptotically $\epsilon_b/t \rightarrow 12\Gamma$. For the same reasons as in the polaron case, namely change of the vacuum with t and screening effects of the other band electrons,

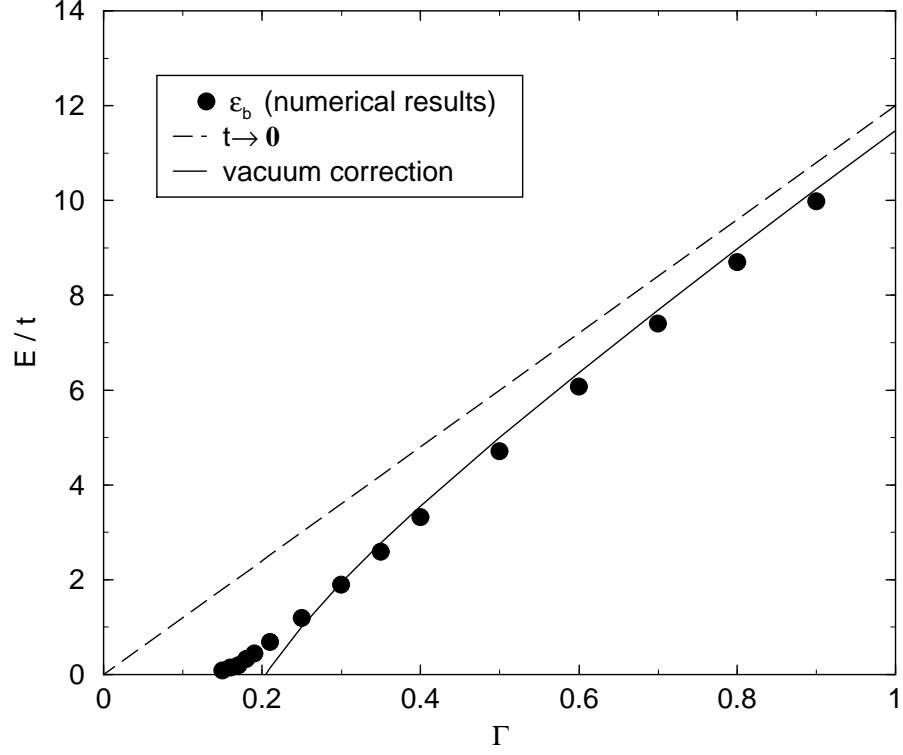


Figure 4.2: Bipolaron lattice relaxation energy ϵ_b

no simple perturbative formula can be used to describe the behavior in the range $\Gamma < 1$. Since in the bipolaron case the gap state is not occupied by electrons, the released energy for the bipolaron state is given by the reduction of the elastic energy costs ΔE_L , if changes in ΔE_e due to the other band electrons are neglected. Therefore, a simple inclusion of a vacuum correction in Eq.(4.10) leads to :

$$\epsilon_b/t = 12\Gamma - \frac{1}{2\Gamma}. \quad (4.20)$$

The agreement of this formula with the numerical values is quite good. However, just introducing a vacuum correction in Eq.(4.10) is not the true story. The analysis of ΔE_L and ΔE_e shows once again, that both terms behave opposite in the studied Γ -range to what is expected from simple perturbative arguments. And again these deviations almost cancel each other and thus account for the fair agreement between numerics and fit.

Polaron versus bipolaron formation

The bipolaron binding energy B_b is twice as big as B_p in the $t = 0$ limit. The reason for the enhanced stability of the bipolaron state lies in the different electronic spectra. Although at $t = 0$, two separated polaron gain more lattice relaxation energy back, two mid-gap states are occupied with one electron each. This state is left empty in the bipolaron case. The neglected Coulomb repulsion will destabilize the bipolaron and postpone the onset of bipolaron formation, and thus polarons could be in principle energetically favorable.

With decreasing electron-phonon coupling strength the ratio between the binding energies $\frac{B_b}{B_p}$ increases, indicating the relative enhanced stability of the bipolaron state compared to the polaron, which is also reflected in the smaller coupling strength required for stability.

4.3.3 Analysis: continuous transition from a small to large polaron

Besides the problem of the vacuum, the difficulties in obtaining easy formulas for the binding energies are caused by screening effects of the other electrons.

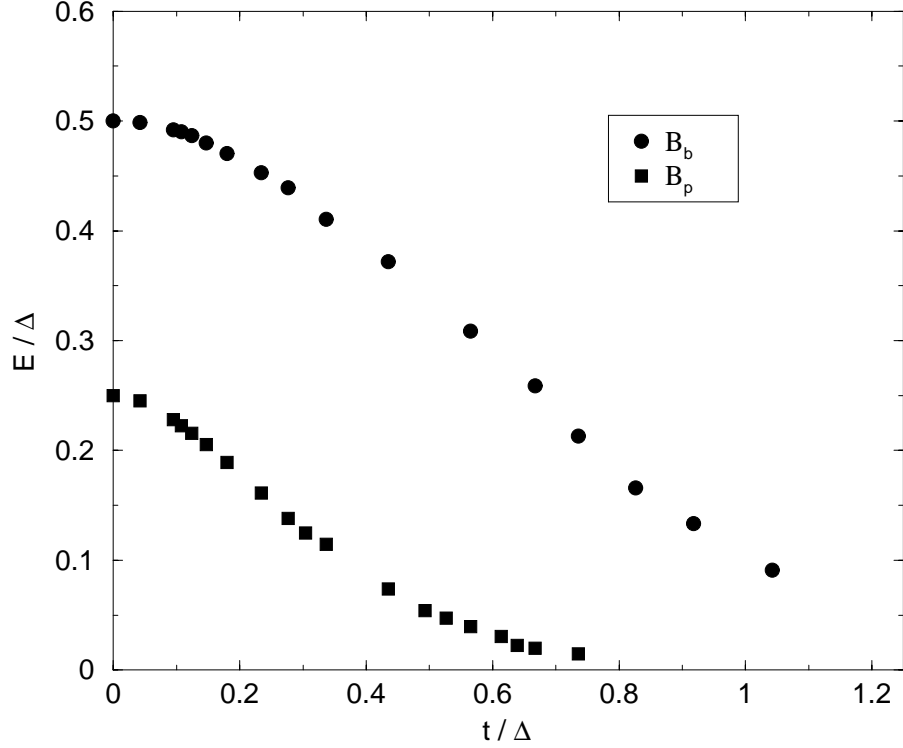


Figure 4.3: Polaron and bipolaron binding energies normalized to the gap Δ

Thus, we study both, single particle and many body properties of the self-trapped states.

A. Many-body properties

To characterize the self-trapped solutions and examine changes with the coupling strength, we analyze the charge distribution by computing and comparing the charge expectation values of the ground- and (bi)polaron state.

Aa. Charge on the center of the (bi)polaron

Self-trapping implies that the inserted hole charge density gets localized on a Bi-atom. In the $t = 0$ limit the hole(s) sit(s) on exactly one site. Fig: 4.4 shows the effect of hopping. It displays the Γ dependence of the maximum amount of hole charge ρ_{center} that is localized on the center of the (bi)polaron positioned at \vec{r}_0 :

$$\rho_{\text{center}} = \sum_i^{\text{occ}} |V_j(\vec{r}_0)|^2 - \sum_i^{\text{occ}} |\Psi_i(\vec{r}_0)|^2, \quad (4.21)$$

where V and Ψ denote the single particle states for vacuum- and (bi)polaron state, respectively and the sum runs over all occupied states.

For the polaron the removed charge density from the central site is close to one for $\Gamma > 0.35$. In the bipolaron case, the maximum charge density $1 + \rho_0$ is removed from an A site, if Γ exceeds 0.4. For smaller Γ , the localized charge density ρ_{center} decreases rapidly, indicating a more delocalized character of the solutions. This behavior is hardly surprising, since it basically reflects a vacuum state property. In Sec.(3.4.2) two critical coupling constants $\Gamma_{c1} = 0.167$ and $\Gamma_{c2} = 0.33$ were assigned to the vacuum marking the transition where the electronic and the total energy per atom, respectively are dominated by the electron-phonon term, i.e. the charge localizing term. This assignment still holds for the lightly doped material and manifests itself in the behavior of the self-trapped states. Around Γ_{c2} ρ_{center} starts to decrease rapidly, around Γ_{c1} the self-localized hole states finally become unstable.

The transition occurs rather quickly. The numerical values for ρ_{center} at the last stable numerical points set an upper limit of 0.3 for the polaron and 0.8 for the bipolaron, respectively. These results further support a second versus a first order transition with Γ into the small (bi)polaron state. The

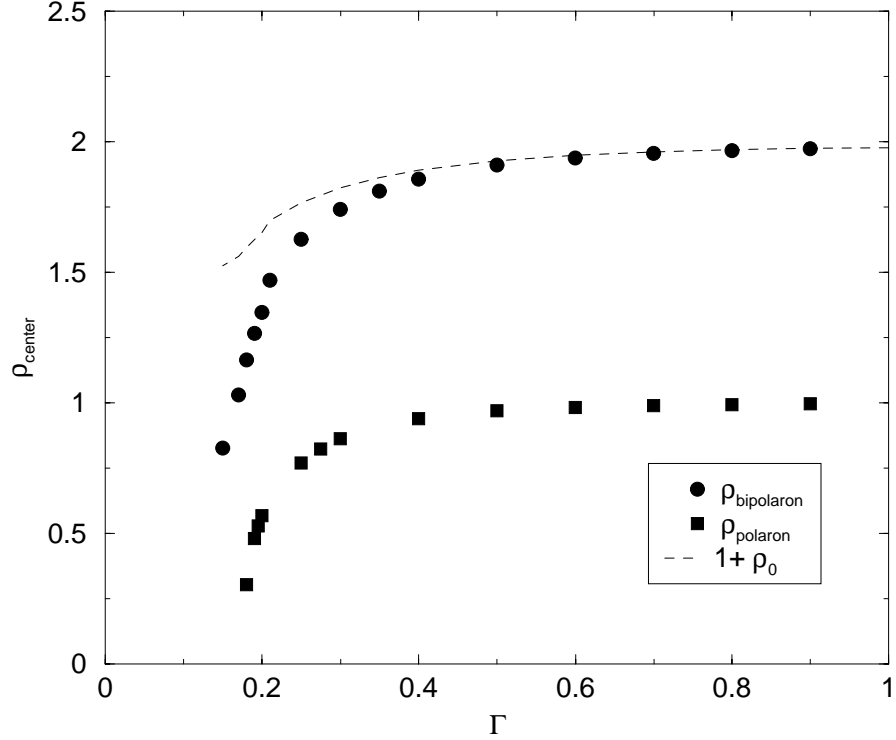


Figure 4.4: Charge localized on the center of the (bi)polaron

initial degree of localization at Γ_c is probably close to zero. One is tempted to compare the transition to the behavior of an electron in a 3D potential well. At a critical depth of the potential well the electron gets bound and the wave function changes phase from a real to an imaginary one. Nevertheless, the probability of finding the electron within the well is still close to zero. In any case, the initial degree of localization in the half-filled band is much less than in the first-order empty band case where 90% of the charge density is concentrated on one site [47].

Ab. Induction of excess charge

The question arises how and where the remaining hole charge density is distributed. A reasonable first guess could be on the next neighbor sites. This, however is only true for very big coupling constants, e.g. $\Gamma > 2$ for bipolarons.

In the previous chapter we showed how the system balances hopping and electron-phonon terms in the vacuum-state by an incomplete charge disproportion. How does a compromise look in the present case? The delocalized hole solutions reduce the gap, i.e. they weaken the charge-density wave, which could be formally interpreted as the creation of an anti-charge density wave. This behavior might get reflected in the (bi)polaron solutions, i.e. the localized hole could attract electrons on the neighbor sites, which themselves attract holes and so on. This means, that on some sites the charge of the (bi)polaron state should be bigger than in the vacuum state.

As a first check, we calculate the total amount of excess charge in the (bi)polaron state ρ_{ind} given by:

$$\rho_{\text{ind}}^{\text{pos}} = \sum_l \delta\rho(r_l) \quad (4.22)$$

where the sum runs over all sites r_l with excess charge, i.e. sites satisfying:

$$\delta\rho(r_l) = \sum_i^{\text{occ}} |\Psi_i(r_l)|^2 - \sum_j^{\text{occ}} |V_j(r_l)|^2 > 0. \quad (4.23)$$

In fact, the insertion of the hole(s) induces a redistribution of negative charge as seen in Fig: 4.5. The total induced negative charge increases with decreasing coupling strength and a power-law behavior was found numerically:

$$\rho_{\text{ind}}^p \propto \Gamma^{-2} \quad (4.24)$$

$$\rho_{\text{ind}}^b \propto \Gamma^{-4}, \quad (4.25)$$

valid for $\Gamma > \Gamma_{c2}$. For weaker coupling the induction effect gets further enhanced.

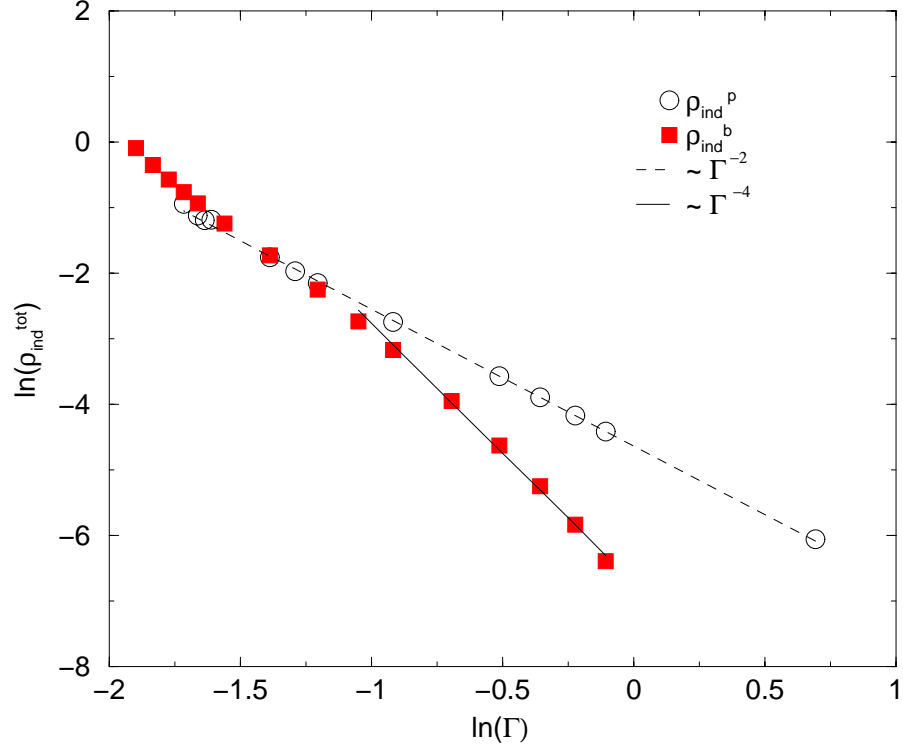


Figure 4.5: Total induced excess charge

Ac. Exponentially damped anti-charge-density waves

What is left is to analyze the spatial redistribution of the charge density to check the hypothesis of a CDW-character of the (bi)polaron and determine their size.

Fig: 4.6 clearly demonstrates the CDW character. Positive and negative

excess charge $\delta\rho$ alternate with distance r from the center of the (bi)polaron. The charge decays exponentially with same decay length λ for positive and

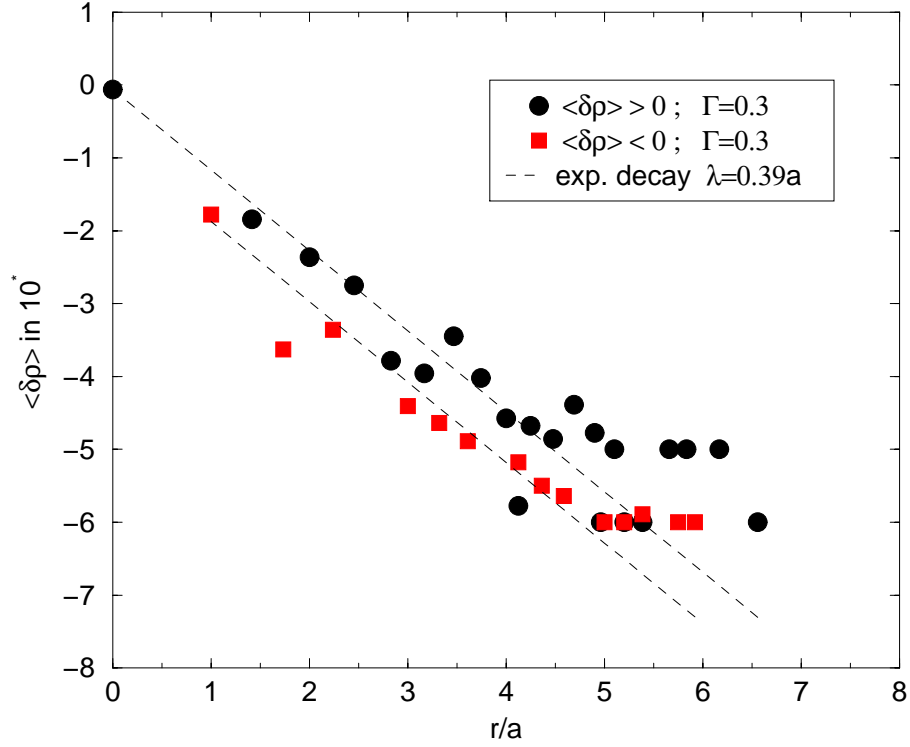


Figure 4.6: Exponential decay and CDW-character of the polarons

negative excess charge. Deviations from the exponential decay at larger distances can be attributed to a finite size effect.

Tab.(4.1) shows the results of least square fits to an exponential decay of the hole charge:

$$\rho(r) = \rho_{\text{center}} \exp\left(-\frac{r}{\lambda}\right). \quad (4.26)$$

Γ	λ_p/a	ρ_{center}^p	λ_b/a	ρ_{center}^b
0.9	0.21	0.99	0.20	1.97
0.6	0.24	0.98	0.23	1.94
0.3	0.39	0.84	0.32	1.74
0.2	0.57	0.58	0.41	1.40

Tab:4.1 Refined decay lengths λ and central charges ρ_{center}

The order of magnitude of the decay length λ is a fraction of the lattice parameter a . It is increasing with decreasing coupling constant and is bigger for a polaron than for a bipolaron. The increasing degree of delocalization of the solution with decreasing Γ is reflected both in the increase of λ and the decrease of ρ_{center} . For $\Gamma > \Gamma_{c2}$, ρ_{center} stays close to its maximum value and the decay length is fairly small. We therefore conclude, that the (bi)polarons are “small” (bi)polarons. The size of the polaron solution below Γ_{c2} is increasing rapidly and evolves continuously into a “large” charge-density-wave-like polaron-solution.

The increasing size of the (bi)polaron is reflected in exponentially decaying displacements of more distant oxygens. This finally explains the behavior of ΔE_L and ΔE_e with Γ . In Sec.(4.3.2) we pointed out that from simple perturbative arguments we would expect ΔE_e to decrease and ΔE_L to increase with decreasing coupling. However, numerics yields the opposite. A polaron or bipolaron solution in a half-filled band corresponds to a localized fast-decaying anti-charge-density-wave. It is accompanied by corresponding lattice distortions, that undo the Peierls distortion. Therefore the number of oxygens that partly relax is increasing with increasing size of the density-wave-like (bi)polaron. This leads to an additional contribution to the lattice

relaxation energy ΔE_L . On the other hand, the energy levels of some band electrons get shifted to higher energies. This is the reason for the increase in ΔE_e .

B. Single particle spectrum: appearance of localized gap-states

Accompanying the (bi)polaron solution are other localized states in the energy spectrum. A total of up to seven gap-states appears in the energy spectra of polaron and bipolaron. Their nature can be understood most easily starting from the $t = 0$ limit. The hole(s) get(s) localized on one site and the surrounding six oxygens relax to their new equilibrium positions. Therefore, the on-site energy (this is the eigen-energy value when $t = 0$), given by the electron-phonon term, changes for seven sites. The site where the hole is localized has its energy increased from $-\Delta = -6gu_0$ to $-\frac{\Delta}{2} = -6g\frac{u_0}{2}$ for the polaron and to 0 for the bipolaron. Their six next-neighbor sites have their energy lowered from Δ to $\frac{11}{12}\Delta = g(5u_0 + \frac{1}{2}u_0)$ and from Δ to $\frac{5}{6}\Delta$ respectively. Thus, if $t \rightarrow 0$, we obtain seven gap states: one splits up from the valence band and six degenerate split down from the conduction band.

Hopping partly lifts the degeneracy and shifts the gap states back towards the conduction- and valence band. The numerical results are shown in Fig.(4.7). For the s gap states a simple perturbative calculation can be done, which agrees fairly well with the numerical results. Due to the localized nature of the polaron we can restrict ourselves to the truncated 7x7 Hamiltonian corresponding to the hole site and its six neighbor sites. We choose a site representation and denote the site of the (bi)polaron by $|0\rangle$ and the surrounding places by $|+x\rangle$, $|-x\rangle$, $|+y\rangle$, $|-y\rangle$ and $|+z\rangle$, $|-z\rangle$. The truncated matrix consists of six non-zero off-diagonal matrix elements, the coupling of $|0\rangle$ to its

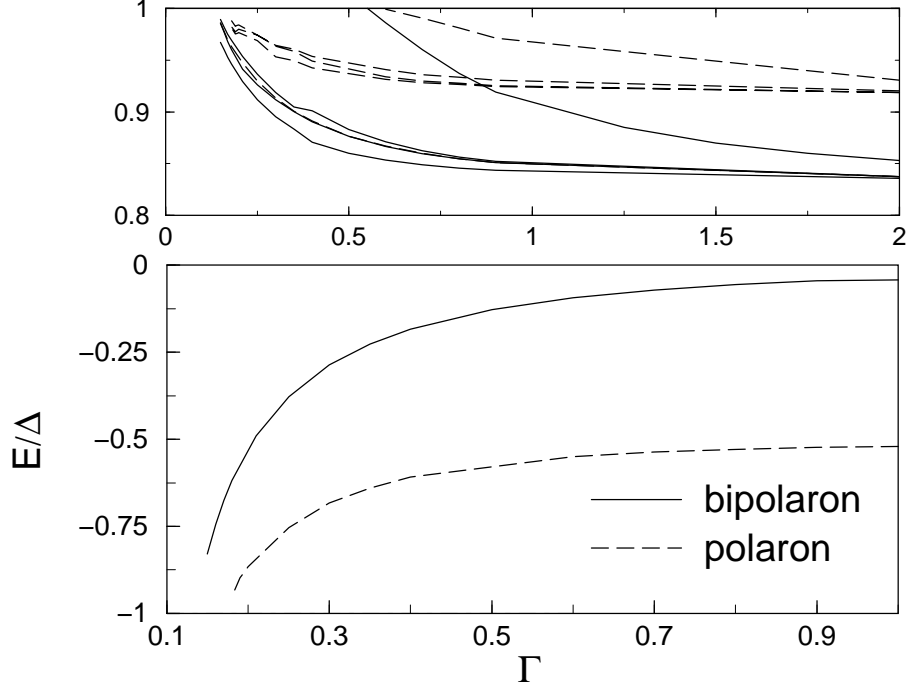


Figure 4.7: Gap state energy dependence on Γ

next neighbors by hopping, and the diagonal matrix elements, given by the electron-phonon term.

In this basis set, the exact eigenstates of truncated Hamiltonian consist of three p-states:

$$|p_i\rangle = \sqrt{\frac{1}{2}}(|+i\rangle - |-i\rangle) \text{ for } i = x, y, z \quad (4.27)$$

and two d-states:

$$|d_{x^2-y^2}\rangle = \frac{1}{\sqrt{4}}(|+x\rangle + |-x\rangle - |+y\rangle - |-y\rangle) \quad (4.28)$$

$$|d_{3z^2-r^2}\rangle = \frac{1}{\sqrt{12}}(2|+z\rangle + 2|-z\rangle) - |+x\rangle - |-x\rangle - |+y\rangle - |-y\rangle. \quad (4.29)$$

Furthermore, for $t = 0$ we can construct two s -states:

$$|s\rangle = |0\rangle \quad (4.30)$$

$$|s^*\rangle = \frac{1}{\sqrt{6}}(|+x\rangle + |-x\rangle + |+y\rangle + |-y\rangle + |+z\rangle + |-z\rangle), \quad (4.31)$$

which are only eigenstates when hopping is neglected.

The truncated Hamiltonian couples for $t \neq 0$ only $|s\rangle$ and $|s^*\rangle$ according to $\langle s|H|s^*\rangle = \sqrt{6}t$. We obtain an effective 2x2 Hamiltonian H_{eff} . The diagonal matrix elements are given by the on-site energies of the polaron site and the next neighbor sites. Once again it is necessary to introduce the vacuum correction, i.e. use the correct u_0 . u_1 can be approximated by $u_1 = u_0 - \frac{g}{k}$, using the fact that the charge removed from the polaron site stays close to 1. Thus, $\langle s|H|s\rangle$ reads:

$$\langle s|H|s\rangle = -6gu_1 = -6g(u_0 - \frac{g}{K}) = -\Delta + 6\frac{g^2}{K} \quad (4.32)$$

and $\langle s^*|H|s^*\rangle$ equals:

$$\langle s^*|H|s^*\rangle = 5gu_0 + gu_1 = \Delta - \frac{g^2}{K}. \quad (4.33)$$

The effective Hamiltonian finally reads:

$$H_{\text{eff}} = \begin{pmatrix} -\Delta + 6\frac{g^2}{K} & \sqrt{6}t \\ \sqrt{6}t & \Delta - \frac{g^2}{K} \end{pmatrix} \quad (4.34)$$

Solving the determinant yields the eigenvalues:

$$\frac{\epsilon_{s,s^*}}{t} = \frac{5}{2}\Gamma \pm \frac{1}{2}\sqrt{(7\Gamma - 2\Delta)^2 + 24}. \quad (4.35)$$

If we include the strong coupling correction for Δ the leading correction to ϵ_s is given by:

$$\frac{\epsilon_s}{t} \longrightarrow -6\Gamma + 0.0891\frac{1}{\Gamma} \text{ for } \Gamma \gg 1 \quad (4.36)$$

or normalized to the gap:

$$\frac{\epsilon_s}{\Delta} \longrightarrow -\frac{1}{2} - 0.0178 \frac{1}{\Gamma^2} \text{ for } \Gamma \gg 1. \quad (4.37)$$

These results agree surprisingly well with the numerical data even for $\Gamma < 1$. The stronger energy shift of the $|s^*\rangle$ -state is due to the fact that this state is coupled to other sites as well.

The results show that the mixing between the s-states is small. This gets certainly reflected in the localization properties of the corresponding wave-functions. The inverse participation ratio (IPR) $\frac{1}{P_i}$ for a state i is defined as:

$$\frac{1}{P_i} = \sum_l |\Psi_i(r_l)|^4, \quad (4.38)$$

where the sum runs over all sites and measures the localization of a state. An IPR of $\frac{1}{P}$ represents a state that is localized on P atoms. The asymptotic values IPR-values for $\Gamma \rightarrow \infty$ for s-,p-,d- and s*-state are given by 1, 0.5, 0.25 and 1/6, respectively, for both, polaron and bipolaron (see 4.27-4.31). With decreasing hopping these states acquire an admixture of more delocalized states and the IPR decreases. The numerical results, presented in Fig:4.8, show the predicted asymptotic behavior with good agreement for $\Gamma > 1$.

These results support and complete the analysis from the previous section. For $\Gamma > \Gamma_{c2}$ the wave-function of the (bi)polaron-state is strongly localized at one site. The energy stays close to $\Delta/2$ and 0 respectively. Below Γ_{c2} the wave-function starts to delocalize and the gap-state energy merges rapidly back into the valence band.

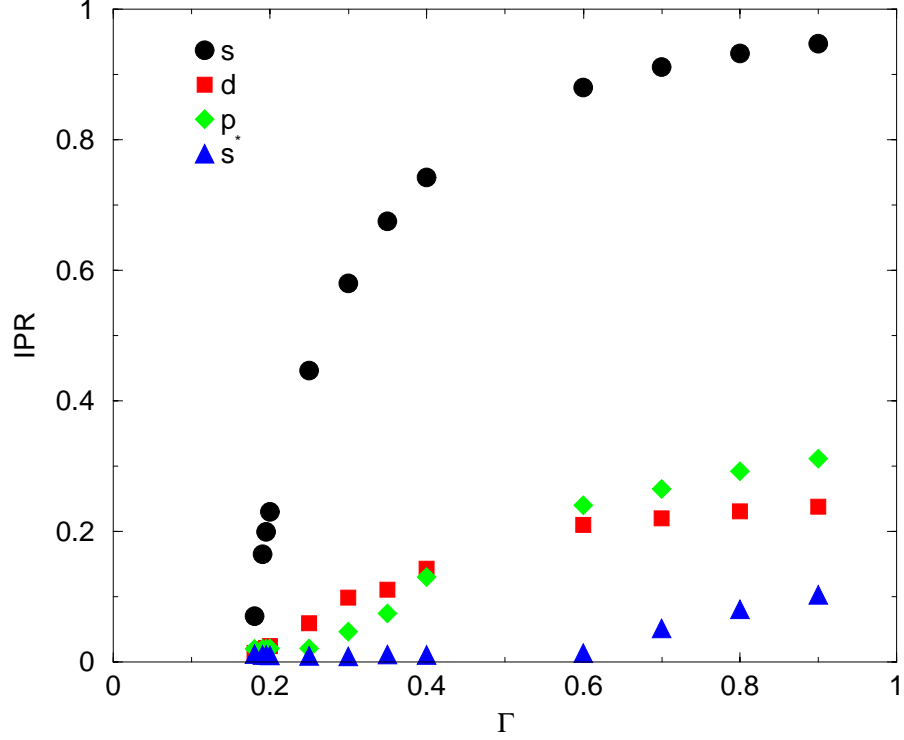


Figure 4.8: Localization of gap states: IPR computed for the polaron

4.4 Summary and conclusions

4.4.1 Toyozawa criterion for self-trapping in the half-filled band

The numerical results yield two kinds of (bi)polaron-like solutions. For coupling constants exceeding $\Gamma \approx 0.35$ the (bi)polaron solutions show the typical properties associated with "small" (bi)polarens. An extremely narrow (bi)polaron-band will form in the gap with energy $\epsilon_p \approx -\Delta/2$ and $\epsilon_b \approx 0$, respectively. The effective mass of the (bi)polarens is very large and the intrinsic

mobility of the self-trapped states is small. Besides, the coherent motion of the holes can be readily destroyed by impurities, e.g. the holes can be further trapped by the acceptor atoms. As a result, incoherent, thermally-activated hopping motion is expected to be the primary motion process.

For $\Gamma < 0.35$, polarons are “intermediate” sized. As Γ decreases their size rapidly increases and the energy of the gap state merges back into the valence band. Screening effects of the other band electrons become very important. These solutions can be described as spherical exponentially-damped charge-density waves. Their mobility will increase with decreasing Γ . Transport and optical properties of the CDW-like polarons in a weak coupling regime should be similar to those of large polarons. Below $\Gamma_c^p \approx 0.18$ and $\Gamma_c^b \approx 0.15$ the polaronlike solutions are unstable.

The stability and the evolution of the polaron solutions for moderate doping in a half-filled band can be predicted by a ”Toyozawa”-criterion [55] in the spirit of Eq.(4.3), i.e. with the idea of competition between localizing and delocalizing terms. The essence of this criterion is that in case of competing terms, the system is in that state which is energetically favorable. Self-trapped, i.e. strongly localized, solutions are stable when the electron-phonon term dominates the total energy of the system. This yields $\Gamma > 2$ (see Eq.(4.4) in the empty band case and $\Gamma > \Gamma_{c2} = \frac{1}{3}$ in the (nearly) half-filled band. For smaller Γ a narrow transition range exists where hopping and electron-phonon term are equally important. In the empty band as well as in the half-filled band the solutions start to delocalize rapidly with decreasing Γ . However, the empty and half-filled cases differ in their ability to compromise between the two competing terms. As soon as the single electron in the empty band starts to delocalize, the oxygen distortion will be smaller, which corresponds to a reduction of the

depth of the trapping potential. This again favors delocalization. Therefore, since the trapping potential is created by the electron itself, the two terms can hardly compromise. This is the reason why there exists only a short branch of metastable solutions. The situation changes in the half-filled band. The depth of the trapping potential can be maintained due to screening effects of the other electrons. The polaron solutions evolve smoothly from small to large polarons and compromise between the two terms by gradually acquiring more delocalized character in terms of CDW-like polarons. The polaron solutions become finally unstable, when hopping starts to dominate E_e , i.e. around $\Gamma_{cl} = \frac{1}{6}$.

4.4.2 Bipolarons in the BBO-system

The results of this chapter suggest that small polaron or bipolaron formation could be the mechanism that accounts for the insulating behavior of BaBiO₃ under moderate doping. Bipolarons are the energetic stable solutions in the RS-model neglecting electron-electron correlations, but polarons could be in principle the energetically favorable quasi-particles. Polaron formation in BaBiO₃ can be excluded from experiment. Measurements of the magnetic properties in doped BaBiO₃ find a large core diamagnetism and provide no indication of isolated spins [9]. This yields a singlet bipolaron state.

The nature of the bipolaron depends on the coupling constant Γ . For BaBiO₃ Γ was estimated in Sec.(3.5.2) to be $\Gamma = 0.3$. The RS-model predicts the stability of small to intermediate sized bipolarons at this coupling strength. The energy of the bipolaron band is slightly shifted from mid-gap towards the conduction band.

The transport data of moderate doped BaBiO₃ reveal a transport gap of 0.24eV [57][58]. This could be consistent with the picture of incoherent motion of bipolarons (Fig.4.9). Thermally assisted hopping occurs via an

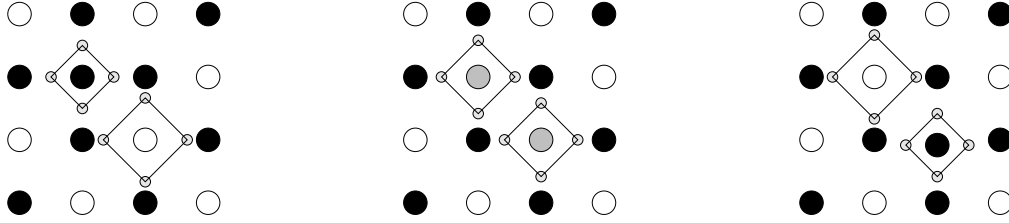


Figure 4.9: Thermally assisted hopping motion of a small bipolaron, black: Bi⁺⁵, white: Bi⁺³, grey: Bi⁺⁴

intermediate state of higher energy [51]. The transfer occurs between sites with equal on-site energy. Thus two sites with the same distortion pattern have to be created as an intermediate state. For small bipolarons the intermediate state with the lowest activation energy has the distortion pattern of two separated polarons and therefore activation energy $\Delta/2$. The activation energy for a polaron would be $\Delta/4$. With the optical gap in BaBiO₃ $2\Delta = 2V$, this would yield an thermal activation energy of 0.5 eV for a small bipolaron model. Since the bipolaron band shifts to the conduction band with decreasing coupling strength, which also diminishes the transport gap, an intermediate sized bipolaron picture could explain the experimental observations.

Further experimental evidence for bipolaron formation comes from tunneling experiments, where a bipolaron model was successfully applied to explain the asymmetric background in the tunneling conductance [59].

Chapter 5

Excitations across the Peierls gap

5.1 Introduction

Theoretical models aim to identify the relevant interactions in a system, that can explain the experimentally observed properties. The charge ordered ground-state of the BaBiO₃-system can be readily explained either on a charge-density Peierls scenario with weak electron-phonon coupling or by strong electron-lattice interaction in a bipolaronic crystal picture. These theories differ in their predictions for the behavior under doping. The first needs some mechanism that allows the gap to stay at the Fermi-energy, e.g. by the formation of incommensurate charge density waves. Whereas with strong electron-phonon interaction, the formation of small polarons or bipolarons is predicted. Another way of revealing the nature of the ground-state is by studying its excitations. The usual probe of excitations in a solid are optical experiments. One

of the first puzzling features, that could not be explained with the simple one electron band-structure, was the existence of distinct peaks below a direct absorption edge in the absorption spectra of many narrow-gap semiconductors. This led to the exciton concept, i.e. to the insight that correlation effects, in form of Coulomb attraction and exchange interaction, between the excited electron and the remaining hole have to be included to describe these excitations accurately. Exciton physics has been studied extensively, exploring the whole range from a large Wannier-Mott exciton to a propagating molecular crystal-excitation in the Frenkel model. However, apart from indirect absorption edges, the role of electron-phonon interaction in the excitation process got little attention. Since the excitons in most narrow gap semi-conductors are extended over the entire crystal, the electron-phonon term only acts as a weak scatterer on the free exciton states and can be neglected. On the other hand, in moderate to large gap insulators the significance of the lattice relaxation processes has now been established in a variety of materials, e.g. rare gas solids, alkali halides, silicon dioxide or organic molecular crystals, just to name some of them [60]. The question how atoms move after the optical excitation and which positions they finally take after relaxation is of considerable interest as it reveals the nature of interatomic forces and thus leads to a better understanding of the ground-state. The theoretical approach in the “traditional” theory of self-trapped excitons is performed on the same footing as small polaron theory and aims to explain line-shape features of exciton-peaks and shifting and line-shape in luminescence spectra [50], [55], [56]. The exciton is treated as a neutral quasi-particle interacting with acoustical phonons in a deformation-type potential. In three-dimensional systems, free and self-trapped states are always separated by a potential barrier. Predominantly free excitons are cre-

ated in the absorption process which tunnel into the self-trapped state, where they further relax [55]. The signature of the relaxation process in these materials is therefore more clearly seen in luminescence than in absorption spectra [60]. BaBiO₃ behaves in many respects different from conventional semiconductors. Optical experiments do not resolve exciton peaks, instead they show a pronounced rather symmetric peak, which is associated with excitations across the Peierls gap. The residual absorption in the gap is not well understood yet. We believe, that relaxation of the oxygens could play a key role to understand the excitations in the BBO system. Thus, the goal of this chapter is to study the nature of the relaxed excited states obtained in the RS-model. We will further neglect Coulomb interaction between hole and electron. Coulomb attraction between the excited electron and hole will primarily lead to an additional energy shift, but the important physics lies in the coupling between the electronic system and the lattice. The term “self-trapped exciton” in the next chapters is used to emphasize the importance of lattice relaxation in the excitation process. The term exciton is meant on a more general basis as it does not deal with alterations caused by direct interaction between hole and electron.

We start in this chapter by briefly contrasting the different kinds of excitations expected for weak and strong electron-phonon coupling in a charge-ordered system. Then the numerical studies on the stability and nature of the self-trapped exciton are analyzed. The impact on the absorption spectra is discussed in the next chapter.

5.2 Low lying excitations in the charge-ordered system

5.2.1 Weak electron-phonon coupling: CDW-picture

An electronic system with a nesting instability at the Fermi energy and which is only weakly coupled to the phonon system, will not self-localize its excitations, analogously to its behavior under doping. This behavior is observed for example in the quasi-one dimensional system $\text{K}_{0.3}\text{MoO}_3$. Besides the single particle excitations across the gap, it has lower lying collective mode excitations. These are difficult to describe within a microscopic theory and are usually treated within a within the framework of time-dependent Ginzburg-Landau theory [24]. Since the order parameter is complex, phase- and amplitude excitations are expected. Both excitations have a gap in case of commensurate CDW's [24]. In an adiabatic limit the amplitude excitation would occur at the gap-energy. However, since the amplitude mode couples to the displacements of the ions, the oscillation frequency is usually smaller than $2\Delta/\hbar$.

If the BBO-system is a three dimensional version of a weak-coupling CDW, similar excitations should be present.

5.2.2 Strong electron-phonon coupling: bipolaronic crystal picture

The idea of a self-trapped exciton evolves naturally from the bipolaronic crystal picture. In the ground-state two electrons are localized on each A -site and one can think of them as electron bipolarons (due to perfect particle-hole symmetry

of the problem, we could choose the holes as well). In this localized view two kinds of excitations are in principle possible:

1. transfer of the bipolaron as a whole from an *A*- to a *B*-site;
2. transfer of an electron to a neighboring *B*-site, leaving formally a hole on the *A*-site.

The energies of these excitations differ roughly by a factor of two. Since the focus of this chapter lies on the low lying excitations, we proceed with a more detailed analysis of the lower energy single-electron transfer excitations.

The excitation and relaxation process

The break-up of an electron pair destroys the balance of the forces acting on the oxygens and changes their rest positions. In a classical picture we expect the oxygens to start to vibrate around these new equilibrium positions. The amplitude of the oscillation, and thus classically the energy residing in the vibrational system, is given by the difference between old and new rest positions. In order to reach the final relaxed excited state, the vibrations have to be damped. The quantum-mechanical analog is not that far away. The excitation process can be described as a simultaneous creation of a charge excitation together with vibrational excitations or phonons. In the Franck-Condon approximation (see Chapter 5) the number of vibrational quanta created is increasing with increasing difference between old and new rest-positions. The local oxygen vibration mode is coupled to other crystal modes and thus allows the oxygens to relax to their new equilibrium positions.

Energy of the relaxed excited state for no hopping

For the $t = 0$ case the energy of the relaxed excited state can be calculated very easily. The relaxed state with the lowest energy is obtained when one electron on the A-site has been transferred to one of the six neighbor sites. A total of eleven oxygens relax, changing the on-site energy of twelve sites. The oxygen-atom connecting the two charge-transfer sites relaxes completely

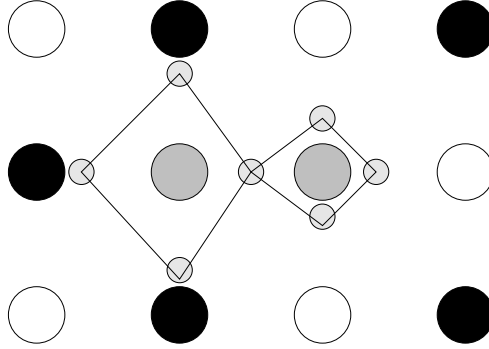


Figure 5.1: The self-trapped exciton, black: Bi^{5+} , grey: Bi^{4+} , white: Bi^{3+}

$u_1 = 0$ and the other ten oxygens relax half-way back $u_2 = \frac{u_0}{2}$. This leads to a reduced elastic energy cost of:

$$\Delta E_L = \frac{K}{2}(-u_0^2 + 10(\frac{u_0^2}{4} - u_0^2)) = -17\frac{g^2}{K}. \quad (5.1)$$

The energy of the remaining electron on the “hole”-site is given by its on-site energy:

$$\epsilon_h = -5gu_2 - gu_1 = -5\frac{g^2}{K}. \quad (5.2)$$

Since the problem exhibits perfect electron-hole symmetry, the energy of the transferred electron is:

$$\epsilon_e = 5gu_2 = 5\frac{g^2}{K}. \quad (5.3)$$

The 5 sites (containing 10 electrons) surrounding the transferred electron have their energy increased from $\epsilon = -6gu_0 = -12\frac{g^2}{K}$ to $\epsilon = -5gu_0 - gu_2 = -11\frac{g^2}{K}$. Compared to the ground-state the electronic energy ΔE_e therefore changes by:

$$\Delta E_e = (\Delta + \epsilon_h) + (\Delta + \epsilon_e) + 10\frac{g^2}{K} = 34\frac{g^2}{K}. \quad (5.4)$$

The total cost of this excitation or the excitation formation energy is:

$$E_{\text{exc}} = \Delta E_e + \Delta E_L = 17\frac{g^2}{K}. \quad (5.5)$$

Without lattice relaxation the minimum excitation energy is given by $2\Delta = 24\frac{g^2}{K}$. This yields a relaxation energy of:

$$\epsilon_{\text{exc}} = 2\Delta - E_{\text{exc}} = 7\frac{g^2}{K}, \quad (5.6)$$

and is the binding energy of the self-trapped exciton. Fig.5.2 is an attempt to display the energy dependence of ground and excited state on the amount of lattice distortion. The optimal oxygen positions of both states are smoothly connected by changing a one-dimensional parameter α , where $\alpha = 0$ corresponds to positions of the ground-state and $\alpha = 1$ to those of the excited state. The energy is computed along this path. Both states change quadratically with α . In the initial ground-state oxygen positions at $\alpha = 0$, the states are separated by the gap 2Δ . The relaxed excited state at $\alpha = 1$ has its energy lowered by $\epsilon_{\text{exc}} = 7\frac{g^2}{K}$. Including on-site Coulomb repulsion the energy-curve of the excited state is shifted downwards by the Hubbard U .

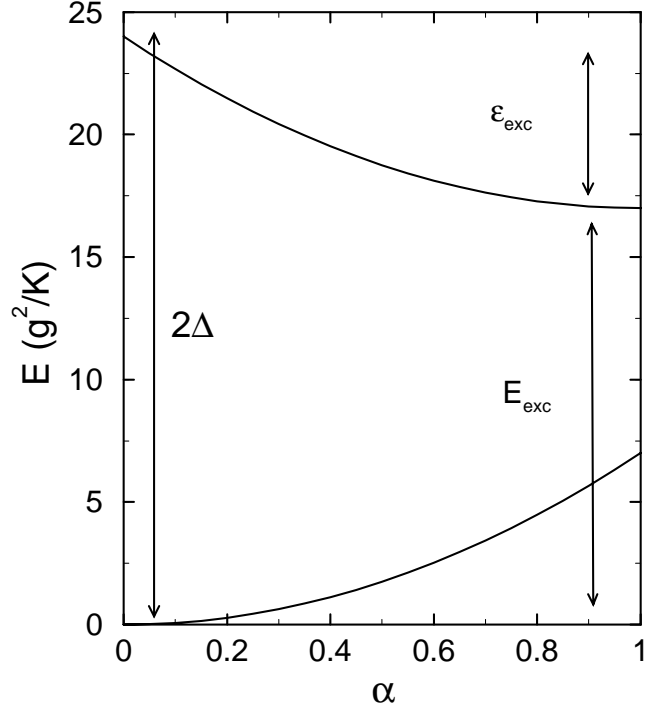


Figure 5.2: Potential energy of ground state and excited state at $t = 0$

5.3 Numerical results

This section studies numerically the stability and nature of relaxed excited states with $t \neq 0$.

5.3.1 Notes on the numerical calculations

In order to find the relaxed excited state with the lowest energy, the total energy of the system is minimized with the algorithm described in chapter 2. One electron is removed from the highest-lying valence band state and inserted into the lowest-lying conduction band state. Then the positions of the oxygens

are varied. Candidate initial oxygen positions are the Peierls ground state solution or the polaron distortion pattern. Cluster size and finite size effects are comparable to those of the polaron calculations (200-400 atoms).

5.3.2 Existence of relaxed excited states

Most of the physics for the self-trapped exciton is the same as in the polaron case. Since perfect electron-hole symmetry occurs, one can think of the self-trapped exciton as an interacting electron-polaron hole-polaron pair, which attract each other.

An energy gain by lattice relaxation was obtained numerically if $\Gamma > \Gamma_c = 0.175$. This is very close to the polaron stability limit ($\Gamma_c = 0.18$). Metastable solutions exist at any $\Gamma > 0.175$, when hole and electron are trapped further apart from each other. Like the polaron, the free state is always unstable when a relaxed state exists. The potential curve of the excited state in Fig.(5.2) has a zero slope at $\alpha = 0$ for $t \neq 0$. However, there is no potential barrier separating the two states along this path. This contrasts with the traditional exciton case [53][56], where a free and trapped state always exist separated by a potential barrier.

The energetics of the self-trapped state and the polaron are almost identical. The changes in the vacuum and screening effects of other band electrons make it difficult to obtain easy perturbative formulas. The numerical calculations show once more a cancellation effect of the nonlinear contributions to ΔE_e and ΔE_L . Thus, the relaxation energy ϵ_{exc} can be approximated quite well by simply inserting the strong coupling formula for Δ Eq.(3.21) into

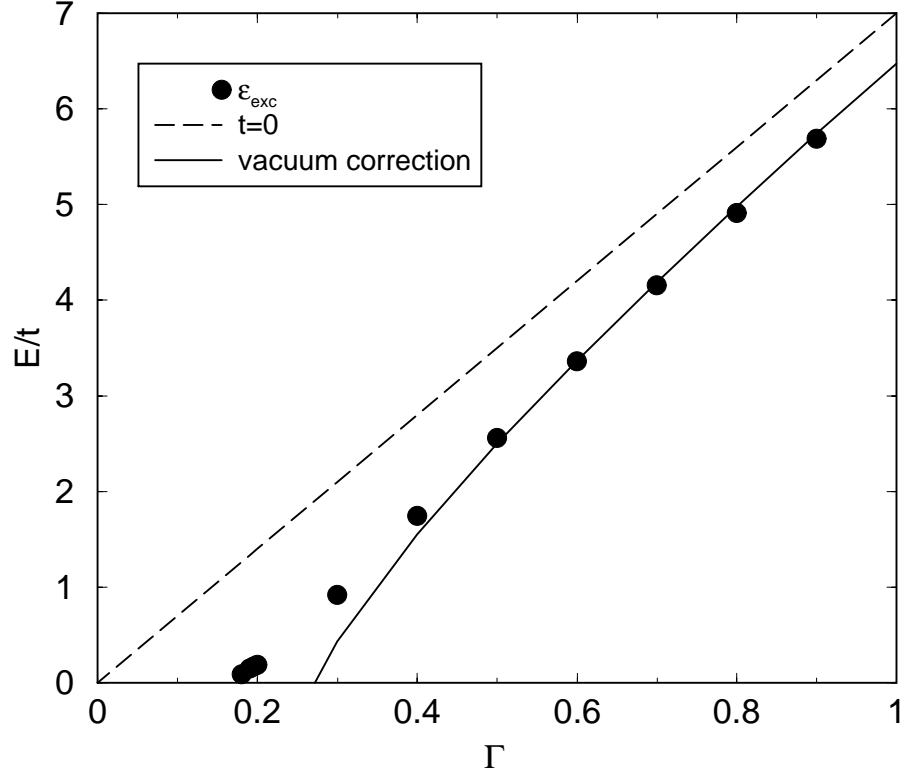


Figure 5.3: Exciton lattice relaxation energy

Eq.(5.6):

$$\frac{\epsilon_{\text{exc}}}{t} \approx 7\Gamma - \frac{1}{2\Gamma}. \quad (5.7)$$

The numerical results are shown in Fig.(5.3). Eq.(5.7) agrees well with the numerical results for $\Gamma > 0.4$ and ϵ_{exc} approaches asymptotically the $t = 0$ limit $7\frac{q^2}{K}$.

5.3.3 Nature of the relaxed excited states

The evolution of the relaxed excited states with Γ is very similar to that of polarons. For sufficient electron-phonon coupling strength, the relaxed excited state is a self-trapped exciton. The self-localized object affects only states in its direct environment. The local change in the oxygen environment leads to the appearance of localized gap states (Fig.(5.4)). Six states emerge from the valence band and six from the conduction band, reflecting the perfect electron-hole symmetry. The five occupied valence band states are slightly shifted by $\frac{g^2}{K}$ and correspond to electrons localized on the sites surrounding the B sublattice site now occupied by the excited electron (called the “exciton-electron” for short). They approach their asymptotic (symmetry determined) IPR values of $\frac{1}{5}$, $\frac{1}{4}$, $\frac{1}{2}$ (doubly degenerate) and $\frac{13}{20}$. Their degeneracy gets partly lifted when they couple to other sites by hopping. The states spread out, as can be seen in the continuous evolution of their IPR-values in the inset in Fig.(5.5), and their energies shift toward the valence band. The same is true for the two states occupied by the exciton-hole and exciton-electron. We calculated the mean radius $\langle r \rangle$ of these two states, shown in Fig.(5.5). A radius of 0 corresponds to the complete localization of the wave-function at one site. The particles are confined approximately to one site for $\Gamma > 0.4$. For $\Gamma < 0.4$, they delocalize rapidly, as indicated by the diverging radius. The finite value at Γ_c is close to the finite system size of the numerical calculations. It should be clear that a delocalized exciton cannot create a trapping potential by itself, since the time spent at one site is too short to cause the oxygens to move. The stability of these spread-out relaxed states is maintained by screening of other band electrons. The self-trapped exciton therefore evolves smoothly into a localized

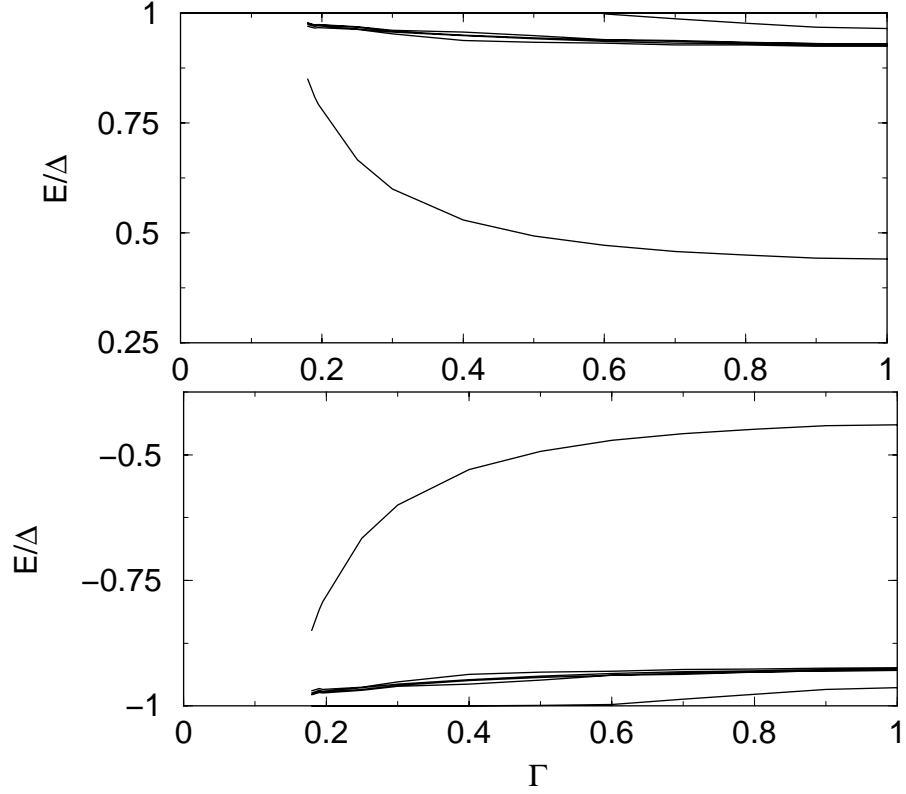


Figure 5.4: Exciton gap states

amplitude excitation of the charge-density wave, like the small polaron was evolving into a large CDW-like polaron.

5.4 Conclusions

The Rice-Sneddon model exhibits two kinds of relaxed excited states depending on the coupling strength Γ , and reflecting the competition of localizing and delocalizing terms in the Hamiltonian. The relaxed excitations in the coupling

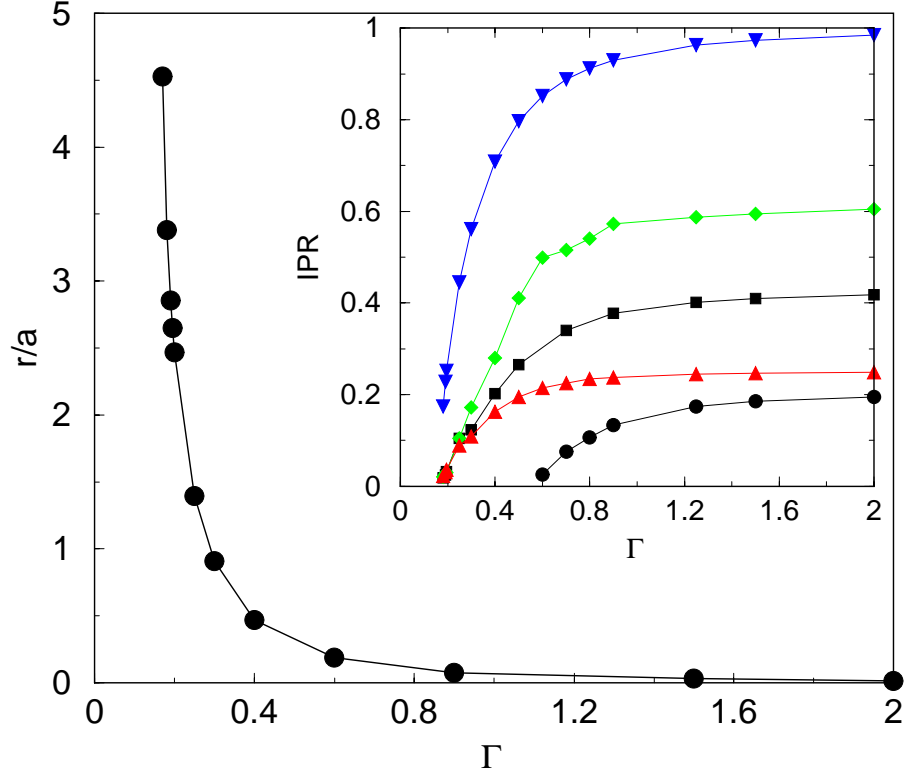


Figure 5.5: Radius of exciton-hole and exciton-electron wave function and IPR's of the gap states

range of bipolaronic crystal $\Gamma > \Gamma_{c2}$ are self-localized excitons. They are most easily understood as a break-up of a crystal-bipolaron with subsequent lattice relaxation.

In the transition range between a bipolaronic crystal and a CDW-system, the relaxed excited states show the signature of localized amplitude excitations of the CDW-ground state. Their benefit from relaxation ϵ_{exc} is small. Thus non-adiabatic effects, which are not treated in our model, will also enter.

Finally, below $\Gamma < 0.175 \approx \Gamma_{c1}$ the adiabatic approximation will definitely fail. Besides the single particle excitations across the gap, collective mode excitations, similar to the one-dimensional weak-coupling CDW-systems, should exist.

Chapter 6

Manifestation of self-trapped states in experiment

6.1 Introduction

The previous chapters analyzed the competition between hopping and electron-phonon term with respect to dopants and with respect to excitations. Self-trapped states are stable if the electron-phonon term exceeds a certain strength. BaBiO₃ has an electron-phonon coupling strength which is large enough for excitons to self-trap, but not quite in the electron-phonon dominated regime where single-site approximation is accurate. It is the aim of this chapter to relate the microscopic theory of self-trapped states to experiment. Optical experiments provide a good opportunity to compare experiment and theory. The optical properties of a material are described phenomenologically by the dielectric function $\epsilon(\omega) = \epsilon_1(\omega) + i\epsilon_2(\omega)$, which can be extracted from experimentally accessible quantities like the absorption coefficient, the reflectivity or

the optical conductivity. The microscopic theory on the other hand provides expressions for the number of transitions induced by light with frequency ω , and thus allows to compute the imaginary part of the dielectric function. Since real and imaginary part are related by the Kramers-Kronig relation, the entire behavior is determined once ϵ_2 is known.

6.2 The half-filled band

The absorption process in solids is complicated and is influenced by many factors. This requires to introduce some level of simplification for computation. One criteria to check whether the important physics was included in a model, is the comparison of the line shape of ϵ_2 between theory and experiment. In many solids the line shape is dominated by the joint-density of states. Therefore we first discuss in this section the density of states effect in the Rice-Sneddon model without taking self-trapped exciton formation into account. Then we analyze the changes predicted due to strong lattice polarization, and briefly discuss other experiments in which a signature of a self-trapped exciton is expected.

6.2.1 DOS-effect

In the simplest approximation only linear absorption in electric-dipole approximation is taken into account, and any lattice or Coulomb interaction polarization effects are neglected. The incoming light induces vertical transitions of electrons in the valence band with energy $E_v(\vec{k})$ into states in the conduction band with same \vec{k} and energy $E_c(\vec{k})$. Since the dipole-matrix element usually changes smoothly with \vec{k} , except at certain k-points where the transition

is forbidden by symmetry, the basic behavior of ϵ_2 is dominated by critical points, i.e. divergences, in the joint-density of states $D_j(\omega)$:

$$D_j(\omega) = \int_{BZ} \frac{2d^3\vec{k}}{(2\pi)^3} \delta(E_c(\vec{k}) - E_v(\vec{k}) - \hbar\omega). \quad (6.1)$$

The simplicity of the Rice-Sneddon model allows to include expressions for the dipole-matrix elements in the computation of ϵ_2 . Vertical transitions between the lower $\vec{k}-\rangle$ and upper Peierls band $\vec{k}+\rangle$ occur at energies:

$$E_c - E_v = \epsilon_{k+} - \epsilon_{k-} = 2\sqrt{\epsilon_k^2 - \Delta^2}, \quad (6.2)$$

with ϵ_k is given by Eq.(3.1).

The dipole-matrix element for transitions between these states can be evaluated using the expression for the momentum matrix elements in site representation:

$$\langle \vec{l} \pm a\hat{j} | \hat{p}_j | \vec{l} \rangle = \pm \frac{ta}{i\hbar} \text{ for } j = \hat{x}, \hat{y}, \hat{z} \quad (6.3)$$

and

$$\langle \vec{l}' | \vec{p}_j | \vec{l} \rangle = 0 \text{ otherwise.} \quad (6.4)$$

This yields:

$$\begin{aligned} \langle k - | \hat{p}_x | k + \rangle &= \frac{1}{N} \sum_{l,l'} e^{ik_x(l-l')a} \langle l' | \hat{p}_x | l \rangle \\ &= \frac{ta\hat{x}}{\hbar i} (e^{ik_x a} - e^{-ik_x a}) = \frac{2ta}{\hbar i} \sin(k_x a). \end{aligned} \quad (6.5)$$

For unpolarized light we therefore obtain for ϵ_2 :

$$\begin{aligned} \epsilon_2(\omega) &= \frac{4e^2 t^2}{m^2 \omega^2 \pi \hbar^2} \int_{BZ} d^3\vec{k} (\sin^2(k_x a) + \sin^2(k_y a) + \sin^2(k_z a)) \\ &* \delta(2\sqrt{\epsilon_k^2 - \Delta^2} - \hbar\omega) \end{aligned} \quad (6.6)$$

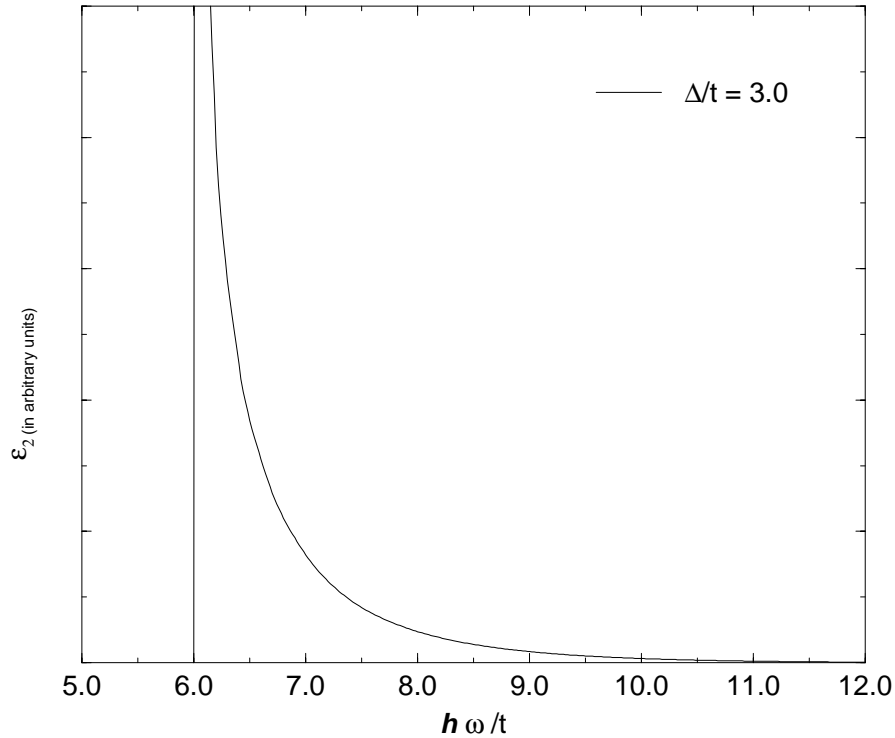


Figure 6.1: ϵ_2 in the RS-model without taking lattice polarization effects into account

This integral can be evaluated numerically with a tetrahedron code[30][31]. Results corresponding to $\frac{\Delta}{t} = 3$ are shown in Fig.6.1. The overall behavior of ϵ_2 is clearly dominated by the divergence of the joint-density of states at incident frequencies $\omega = \frac{2\Delta}{\hbar}$. The peak corresponds to transitions from states at the top of the lower Peierls band into those at the bottom of the upper band. These states however are mainly responsible for the charge disproportion and have vanishing amplitude on the A and B sites respectively. The larger the electron-phonon coupling strength is, the more easily can their phase coherence be destroyed. This means that these states tend to localize. Excitations

created in transitions between localized states, on the other hand, self-trap very easily. Thus, since transitions between these states are highest in density we expect the overall line shape to be dominated by the signature of self-trapped excitons.

6.2.2 Franck-Condon effect: signature of the ST-exciton

The Franck-Condon principle

Materials with self-trapped excitons show Franck-Condon-type broadening of the electronic transition. The Franck-Condon effect is well known among molecular spectroscopists. Molecular excited electronic states generally have altered atomic coordinates. Thus, the excitation process can be described as a simultaneous creation of an electronic excitation and nuclear vibrations. This leads to the appearance of Franck-Condon multivibrational sidebands in the electronic spectra [61]. In simple solids, excitations are usually delocalized which eliminates this effect [56]. However, in case of self-localized states, because of their significant lattice relaxation, Franck-Condon-type broadening of the electronic transitions must reappear.

The Franck-Condon principle has its physical origin in the fact that the electronic transition occurs on a time scale that is several orders of magnitude shorter than the period of the atomic vibration, in agreement with the assumptions behind the Born-Oppenheimer separation. This means that the positions of the atoms R during an electronic transition $\lambda \rightarrow \lambda'$ do not change. The wave function $\Phi_{\lambda n}(r, R)$ of the electron-phonon system corresponding to the energy $E_{\lambda, n}$, can be factorized in an electronic $\psi_{\lambda}(r, R)$ and a vibrational $\chi_{\lambda n}(R - R_{\lambda})$ part. ψ_{λ} is the solution with energy $\epsilon_{\lambda}(R)$ to the Schrödinger

equation for an electron in the potential of the atoms characterized by the adiabatic parameter R , and $\chi_{\lambda n}(R - R_\lambda)$ is the solution for the atomic vibrations in the potential $W_\lambda(R) = U(R) + \epsilon_\lambda(R)$.

The dipole matrix element $P_{\lambda n \lambda' n'}$ therefore can be written as:

$$P_{\lambda n \lambda' n'} = \int dR \chi_{\lambda n}(R - R_\lambda) \chi_{\lambda' n'}(R - R_{\lambda'}) \int dr \psi_\lambda(r, R) \hat{P} \psi_{\lambda'}(r, R) \quad (6.7)$$

This integral can be large even when the vibrational quantum numbers n , n' are quite different from each other, because the vibrational wave-functions $\chi_{\lambda n}$, $\chi_{\lambda' n'}$ are off-set from each other. The second integral in Eq.(6.7) depends in general on R , but neglecting it is a standard approximation and should not cause much error. Vibrational transitions have intensities governed by the Franck-Condon factor $\langle \lambda n | \lambda' n' \rangle = \int dR \chi_{\lambda n}(R - R_\lambda) \chi_{\lambda' n'}(R - R_{\lambda'})$. Those transitions are the most probable, whose probability maxima of the vibrational wave function occur approximately at the same R . This however, depends only on the relative shifts in $R_\lambda - R_{\lambda'}$ of the of the adiabatic potentials $W_\lambda(R)$ and $W_{\lambda'}(R)$.

Temperature enters the absorption, since in thermal equilibrium the ensemble of the system is distributed over vibronic states λn with probabilities $w_{\lambda n}$. As long as the thermal energy $k_B T = \beta^{-1}$ is much smaller than the energy separation between the electronic ground state (λ) and excited (λ') states, the system is certainly in the electronic ground state, and the optical absorption for light with frequency ω corresponding to the electronic transition is proportional to:

$$\epsilon_2(\omega) \propto |P_{\lambda \lambda'}|^2 \sum_n \sum_{n'} w_{\lambda n} |\langle \lambda n | \lambda' n' \rangle|^2 \delta(\hbar\omega + E_{\lambda n} - E_{\lambda' n'}) \quad (6.8)$$

Franck-Condon effect for the ST-exciton

At zero temperature, the broadening of the electronic transition comes from the zero point motion of the oxygens and the sum over n in Eq.(6.8) has only one term, $w_{\lambda n} = \delta_{n,0}$. The excited electron states, in single site-approximation, couple to eleven oxygens, which are treated as independent Einstein oscillators with frequency ω_0 and oxygen mass M in our model. They move in harmonic potentials and thus the vibrational wave function for initial and final state can be written as a product of the 11 wave functions corresponding to oscillators. The wave function of an oscillator in the ground state takes the form $\chi_{\lambda 0}(R) = \exp(-\frac{M\omega_0}{\hbar}(R - R_\lambda)^2)$ and in the excited state $\chi_{\lambda' n}(R) = H_n(R - R_{\lambda'}) \exp(-\frac{M\omega_0}{\hbar}(R - R_{\lambda'})^2)$, where H_n is a Hermite polynomial of order n and $R_\lambda, R_{\lambda'}$ are the rest positions of the oscillator in initial and final state, respectively. The energy difference between initial and final state is given by the exciton formation energy E_{exc} plus the total number n of vibrational quanta created on the 11 oxygens:

$$E_{\lambda 0} - E_{\lambda' n} = E_{\text{exc}} + n\hbar\omega_0. \quad (6.9)$$

The Franck-Condon factor is a product of eleven vibrational overlap integrals of the form $|\langle 0|n_i\rangle|^2$ with:

$$\langle 0|n_i\rangle = \left(\frac{\alpha^2}{2}\right)^{\frac{n_i}{2}} \frac{(R_\lambda - R_{\lambda'})^{n_i}}{\sqrt{n_i!}} \exp(-\frac{\alpha^2}{4}(R_\lambda - R_{\lambda'})^2), \quad (6.10)$$

where $\alpha = \sqrt{\frac{M\omega_0}{\hbar}}$. To obtain the total absorption at a frequency $\hbar\omega = E_{\text{exc}} + n\hbar\omega_0$, we have to sum over all different possibilities to distribute n quanta over

the eleven oxygens:

$$\begin{aligned} & \sum_{n_1, n_2, \dots, n_{11}} |\langle 0 | n_1 \rangle|^2 |\langle 0 | n_2 \rangle|^2 \dots |\langle 0 | n_{11} \rangle|^2 \delta\left(\sum_{i=1}^{11} n_i - n\right) \\ &= \left(\frac{E_r}{\hbar\omega_0}\right)^n \frac{1}{n!} \exp\left(-\frac{E_r}{\hbar\omega_0}\right), \end{aligned} \quad (6.11)$$

where E_r is an energy associated with the lattice relaxation:

$$E_r = \frac{K}{2} \sum_{i=1}^{11} (R_i - R'_i)^2. \quad (6.12)$$

For the self-trapped exciton $E_{\text{exc}} = 2\Delta - \epsilon_{\text{exc}} = \frac{17}{12}\Delta$ and $E_r = \frac{K}{2}(10\frac{u_0^2}{2} + u_0^2) = \frac{7}{12}\Delta$. Thus, ϵ_2 is in single-site approximation:

$$\epsilon_2(\omega) = \frac{4\pi^2 e^2}{m^2 \omega^2} \sum_n \frac{1}{n!} \left(\frac{7}{12}\frac{\Delta}{\hbar\omega_0}\right)^n \exp\left(-\frac{7}{12}\frac{\Delta}{\hbar\omega_0}\right) \delta\left(\hbar\omega - \frac{17}{12}\Delta + n\hbar\omega_0\right) \quad (6.13)$$

Fig.6.2 shows the absorption expected with a gap of 2.0eV coupled to phonons with breathing-mode frequency $\omega_0 = 70\text{meV}$. In the idealized case absorption occurs at discretized frequencies corresponding to different numbers of vibrational quanta created in the absorption process. In reality these peaks certainly get broadened and discrete peaks may not be seen in experiment. The overall line shape should look similar to the envelope function of Fig.6.2, with maximal absorption at $\omega = 2\Delta$ and significant absorption in the gap.

For non-zero t we argue according to the DOS-effect described in Sec.(6.2.1). For not too large values of the hopping parameter t (i.e. within the self-trapping regime), the absorption spectra will be dominated by the creation of highly vibrational excited self-trapped excitons with some additional absorption at higher energies corresponding to transitions from states from the bottom of the lower to the top of the upper Peierls band. Since these states are delocalized, they do not self-trap and probably can be treated in a simple

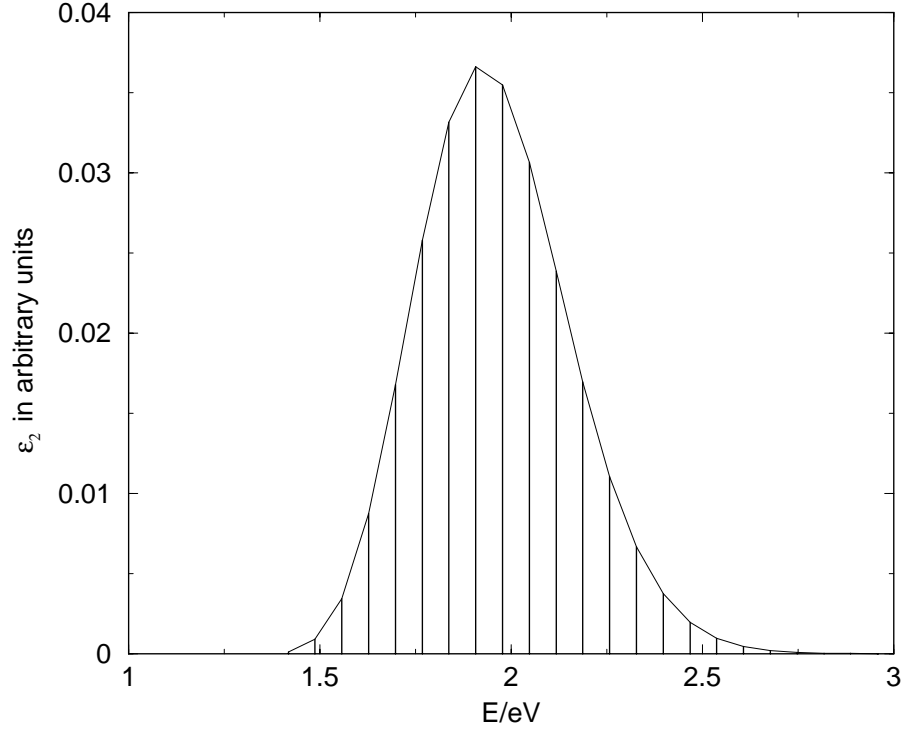


Figure 6.2: Franck-Condon type spectra for the self-trapped exciton

band-to-band transition picture. A unified treatment of band- and Franck-Condon effect would not be easy and we have not succeeded in doing it.

The temperature effect up to room temperature is very weak. At $T = 300\text{K}$ the probability to find a phonon on one of the eleven oxygens is less than 6%. The analytical calculations for temperature corrections become increasingly tedious. Fig.6.3 shows a first temperature correction obtained numerically. Temperature enhances slightly the absorption in the low energy regime and shifts the on-set of absorption to smaller energies.

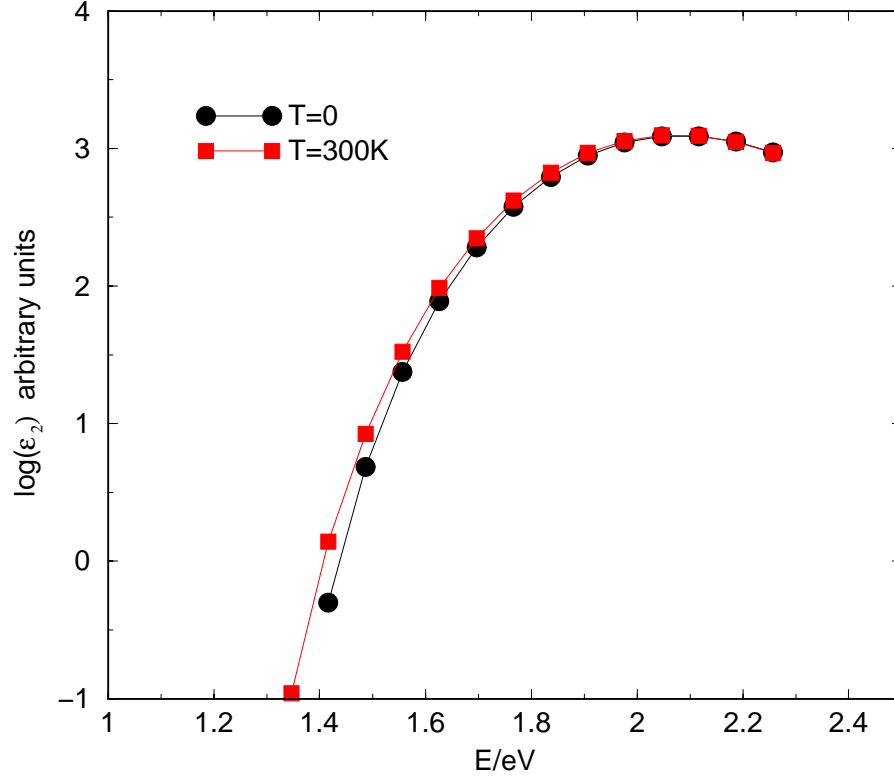


Figure 6.3: First temperature correction to ϵ_2

6.2.3 Experimental impact and comparison to experiment

ST-exciton in the optical conductivity

Numerous optical experiments have been performed on the BBO-compounds. Optical response data in the mid-infrared regime for the undoped material has been published e.g. by Karlow et. al [41], Blanton et al. [42] and Kozlov et al. [62]. The line shape of the optical conductivity is similar to the curve obtained by formation of self-trapped excitons. However, the full width at

half maximum (FWHM) between experiment and the theoretical prediction from our simple model differs by a factor of two (FWHM 1.0V (experiment) compared to 0.5V (ST-exciton)). Besides, there is residual conductivity below 1.4V. Some density functional calculations find an indirect gap [63], which was employed in Ref.[62] to explain the absorption in the gap. However, band theories based on current approximate density-functional procedures tend to underestimate gaps fairly badly and do not give a reliable information about gaps in BaBiO₃. Instead we believe that the residual absorption is caused by local defects in the charge-ordered state through excitations into gap states. Besides Coulomb interaction was not taken into account in our model. This will shift the on-set of absorption.

Coupling between electronic and lattice excitation

Clear experimental support for the creation of self-trapped excitons in BaBiO₃ comes from Raman experiments [43]. The Raman spectra is dominated by an extreme strong peak at 570cm⁻¹, which was assigned to the breathing mode phonon. Contrary to the Raman-effect in usual semi-conductors, a series of higher harmonics is observed. This is consistent with the existence of virtual excited states composed of electronic and vibrational quanta, and thus allows to observe the higher harmonics.

Most excitons created in the absorption process are highly vibrational excited states. Before electron and hole recombine, the exciton relaxes by the emission of phonons. The maxima of the luminescence peak should therefore be red-shifted with respect to the absorption peak. Moreover, a decrease in the differential transmission for energies below 2Δ is expected in time resolved spectroscopy experiments. The first pulse creates highly vibrational excited

excitons. They relax by the emission of phonons and which means that the oxygens relax into their new equilibrium positions. This however, corresponds to the appearance of the gap states below the conduction band, into which electrons can be excited by the second pulse.

To conclude the excitations across the Peierls gap in BaBiO_3 show the signature of self-trapped excitons. However, improvement of our simplest model is necessary to obtain better agreement between the experimental and theoretical optical conductivity curves.

Bibliography

- [1] A.W. Sleight, J.G. Gillson, P.E. Bierstedt, *Solid State Commun.* 17, 27 (1975)
- [2] R.J. Cava, B. Batlogg, J.J. Krajewski, R. Farrow, L.W. Rupp, Jr., A.E. White, K. Short, W.F. Peck, T. Kometani, *Nature* 332, 814 (1988)
- [3] Q. Huang, J.F. Zasadzinski, N. Tralshawala, K.E. Gray, D.G. Hinks, J.L. Peng, R.L. Greene, *Nature* 347, 369 (1990)
- [4] H. Sato, H. Takagi, S. Uchida, *Physica C* 169, 391 (1990)
- [5] B.M. Moon, C.E. Platt, R.A. Schweinfurth, D.J. Van Harlingen, *Appl. Phys. Lett.* 59, 1905 (1991)
- [5] F. Sharafi et al., *Phys. Rev. B* 44, 12521 (1991)
- [6] S. Pei, J.D. Jorgensen, B. Dabrowski, D.G. Hinks, D.R. Richards, A.W. Mitchell, Y. Zheng, B., N.E. Bickers, D.J. Scalapino, *Phys. Rev. B* 40, 6862 (1989)
- [7] H. Sato, S. Tajima, H. Takagi, S. Uchida, *Nature* 338, 241 (1989)
- [8] E.S. Hellmann, E.H. Hartford, Jr., *Phys. Rev. B* 47, 11346 (1993)

- [9] B. Batlogg et al., Phys. Rev. Lett. 61, 1670 (1988)
- [10] B. Batlogg, in *Mechanism of High Temperature Superconductivity*, ed. by H. Kamimura and A. Oshiyama, Springer Series in Material Science Vol. 11 (Springer Verlag Berlin, 1989), p. 324
- [11] B. Batlogg, R.J. Cava, L.W. Rupp, Jr., A.M. Mujsce, J.J. Krajewski, J.P. Remeika, W.F. Peck, Jr., A.S. Cooper, G.P. Espinosa, Phys. Rev. B 61, 1670 (1988)
- [12] D.G. Hinks, D.R. Richards, B. Dabrowski, D.T. Marx, A.W. Mitchell, Nature 335, 419 (1988)
- [13] L.F. Mattheis, D. R. Hamann, Phys. Rev. B 28, 4227 (1983), Phys. Rev. B 26, 2686 (1982)
- [14] L.F. Mattheis, D. R. Hamann, Phys. Rev. Lett. 60, 2681 (1988)
- [15] S. Pei et al., Phys. Rev. B 41, 4126 (1990)
- [16] T.M. Rice, L. Sneddon, Phys. Rev. Lett. 47, 689 (1982)
- [17] P. Prelovsek, T.M. Rice, F.C. Zhang, J. Phys. C 20, L229 (1987)
- [18] W.D. Mosley et al., Phys. Rev. Lett. 73, 1271 (1994)
- [19] A. Muramatsu, W. Hanke, Phys. Rev. B 48, 878 (1988)
- [20] P.B. Allen, V. Kostur, Z. Phys. B 104, 613-618 (1997)
- [21] J. Yu, X.Y. Chen, W.P. Su, Phys. Rev. B 41, 344 (1990)

- [22] W.H. Press, B.P. Flannery, S.A. Teukolsky, W.T. Vetterling, *Numerical Recipes in C* (Cambridge University Press,1988)
- [23] D.A. Papaconstantopoulos, A.Pasturel, J.P. Julien, F. Cyrot-Lackmann, Phys. Rev. B 40, 8844 (1989)
- [24] G. Grüner, *Density Waves in Solids*, Addison-Wesley Publishing Company (1994)
- [25] A.W. Overhauser, Phys. Rev. Lett. 4, 462 (1960) and PR 128, 1437 (1962)
- [26] C.M. Varma, Phys. Rev. B 61, 2713 (1988)
- [27] G. Vielsack, W. Weber, Phys. Rev. B 54, 6614 (1996)
- [28] V. Meregalli, S.Y. Savrasov, Phys. Rev. B 57, 14453 (1998)
- [29] A short review can be found in C. Kittel, *Introduction to Solid State Physics*, 7th edition, John Wiley & Sons Inc. New York (1996), p.300 , a detailed version in Ref. [24]
- [30] G. Lehmann, P.Rennert, M.Taut, H. Wonn, Phys. Stat. Sol. (b) 54, 469 (1972); 57, 815 (1973)
- [31] O. Jepsen, O.K. Andersen, Solid. State Commun. 9, 1763 (1971)
- [32] D.E. Cox and A.W. Sleight, Solid State Commun. 19, 946 (1976)
- [33] G. Thornton, A.J. Jacobson, Acta. Crystallogr. B 34, 351 (1978)
- [34] C. Chaillout, A.Santoro, Solid State Commun. 65, 1363 (1988)

- [35] B. Boyce, F.G. Bridges, T. Claeson, T.H. Gebaelle, G.G. Li, A.W. Sleight, Phys. Rev. B 44, 6961 (1991)
- [36] T.J. Wagener, H.M. Meyer III, D.M. Hill, Y. Hu. M.B. Jost, J.H. Weaver, D.G. Hinks, B. Dabrowski, D.R. Richards, Phys. Rev. B 40, 4532 (1989)
- [37] M. Qvarford et al., Phys. Rev. B 54, 6700 (1996)
- [38] H. Namatme, A. Fujimori, H. Takagi, S.Uchida, F.M. de Groot, J.C. Fuggle, Phys. Rev. B 48 16917 (19)
- [39] A.V. Puchkov, T. Timusk, M.A. Karlow, S.L. Cooper, P.D. Han, D.A. Payne, Phys. Rev. B 54, 6686 (1996)
- [40] S.H. Blanton, R.T. Collins, K.H. Kelleher, L.D. Rotter, Z. Schlesinger, Phys. Rev. B 47, 996 (1993)
- [41] M.A. Karlow, S.L. Cooper, A.L. Kotz, M.K. Klein, P.D. Han D.A. Payne, Phys. Rev. B 48, 6499 (1993)
- [42] P. Blaha, K. Schwarz, G. Vielsack, and W. Weber, in *Electronic Properties of High- T_c Superconductors and Related Compounds*, edited by H. Kuzmany, M. Mehring, and J. Fink (Springer, Berlin, 1990).
- [43] S. Tajima, M. Yoshida, N. Koshizuka, H. Sato, S. Uchida, Phys. Rev. B 46, 1232 (1992)
- [44] S. Tajima, S. Uchida, A. Masaki, H. Tagaki, K. Kitazaw, S. Tanaka, S. Katsui, Phys. Rev. B 32, 6302 (1985)
- [45] G. Vielsack, W. Weber, Physica C 235-240, 2521 (1994)

- [46] U. Hahn, G. Vielsack, W. Weber, Phys. Rev. B 49, 15936 (1994)
- [47] V.N. Kostur, P.B. Allen, Phys. Rev. B 56, 3105 (1997)
- [48] L.D. Landau, Phys. Z. Sowjetunion 3, 664 (1933)
- [49] H. Fröhlich, Adv. Phys. 3, 325 (1954)
- [50] S. Nakajima, Y. Toyozawa, R. Abe, *The Physics of Elementary Excitations*, Springer-Verlag (1989)
- [51] N.F. Mott, E.A. Davis, in *Electronic Processes in non-crystalline Materials*, 2nd Edition (Oxford University Press 1979)
- [52] D. Emin, Phys. Rev. B 48, 13691 (1993)
- [53] Y. Toyozawa, Y. Shinozuka, J. Phys. Soc. Japan 48, 472 (1980)
- [54] T. Holstein, Ann. Phys. (N.Y.) 8, 325 (1959); 8, 343 (1959)
- [55] Y. Toyozawa, *Relaxation of Elementary Excitations*, ed. R. Kubo and E. Hanamura, (Springer-Verlag, 1980)
- [56] E.I. Rashba, *Opt. Spektrosk.* 2, p.75 (1957)
- [57] A. Gosh, Solid State Communications 112, 45 (1999)
- [58] E.S. Hellman, B. Miller, J.M. Rosamilia, E.H. Hartford, K.W. Baldwin, Phys. Rev. B 44, 9719 (1991)
- [59] E.S. Hellman, E.H. Hartford, Jr., Phys. Rev. B 52, 6822 (1995)
- [60] K.S. Song, R.T. Williams, *Self-trapped Excitons*, (Springer-Verlag, 1993)

- [61] G.Herzberg, *Spectra of Diatomic Molecules*, (Van Nostrand, 1950)
- [62] M.E. Kozlov, X. Ji, H. Minami, H.Uwe, Phys. Rev. B 56, 12211 (1997)
- [63] A.I. Liechtenstein, I.I. Mazin, C.O. Rodriguez, O. Jepsen, O.K. Anderson, M. Methfessel, Phys. Rev. B 44, 5388 (1991)